UNIVERSITEIT GENT

FACULTY OF MEDICINE AND HEALTH SCIENCES

Academic Year 2015 - 2016

'Effects of radiotherapy and concurrent VEGF inhibition on tumor microvascular function in a mouse xenograft model'

Bert VERBERCKMOES

Promotor: Prof. Dr. Wim Ceelen

Dissertation presented in the 2nd Master year
in the programme of

Master of Medicine in Medicine

UNIVERSITEIT GENT

FACULTY OF MEDICINE AND HEALTH SCIENCES

Academic Year 2015 - 2016

'Effects of radiotherapy and concurrent VEGF inhibition on tumor microvascular function in a mouse xenograft model'

Bert VERBERCKMOES

Promotor: Prof. Dr. Wim Ceelen

Dissertation presented in the 2nd Master year
in the programme of

Master of Medicine in Medicine

Preface

The accomplishment of this master paper requested many sacrifices and efforts. Difficulties along the tract were encountered and translated into instructive and unique experiences. Thus I present this master paper with big enthusiasm.

I would like to thank Elodie Melssens, PhD student, for her support in writing my master paper. Since she build up large experience by conducting a more integrated study on DSWC and combined radiotherapy and cediranib, her advises were of inestimable value and without her this master paper won't be as structured.

Furthermore I would like to thank the ambitious and hardworking crew of the Gastro-Intestinal experimental laboratory of UZ Ghent for bringing good atmosphere when I was performing the video analyses.

I would like to thank prof. dr. Wim Ceelen for starting me up and providing the essential lecture and generous support to accomplish this master paper.

I want to thank Yannick , my cousin, to scan this paper on correct grammar and spelling. "*Edle Einfalt und stille Grösse"*- Yannick.

Last but not least I would like to thank my parents, Lynn, Steven, Michiel, Leander, Edward, Lukas, Bernard, Seppe and many others for pleasant diversion and support.

TABLE OF CONTENTS

ABSTRACT

Introduction

Colorectal cancer is the second deadliest cancer in Europe. Different mechanisms grant tumors better survival capacities and treatment resistance. Aberrant tumor angiogenesis has shown to induce a hostile tumor environment where metastatic tumor cells flourish and treatment strategies sputter. In preclinical studies cediranib, a potent VEGF receptor inhibitor, has shown to prune immature tumor vessels and normalize the tumor environment. Combining the effects of cediranib to radiotherapy is believed to enhance either vascular normalization or vascular destruction in a dose dependent manner.

Material and Methods:

In this study fractionated radiotherapy (1.8Gy dd) and cediranib were administered concurrently (6mg/kg/d) or as monotherapies. The effects were observed through in vivo fluorescence microscopy in dorsal skinfold window chamber mouse models. To integrate the clinical aim, human colorectal cancer cells (HT29) were engrafted in nude mice. After three days of recovery and observation, the treatment regimen was initiated for 5 consecutive days. 4 treatment groups where designed to either receive vehicle, one modality alone or concurrent modality treatment. Videos were analyzed through imaging software ImageJ and CapImage. To investigate the vascular 'normalization' effects typical tumor vasculature variables were defined: vascular branching, density, diameter, RBC velocity, volumetric flow, tortuosity and permeability.

Results

A reduction in vascular tortuosity comparing the cediranib monotherapy group with the controls group was statistically proven ($P=0.012$). In addition the cediranib group showed the least permeable vessel wall ($P<0.001$), also the concurrent modality treatment group showed a more intact vessel wall ($P<0.001$). Remarkably the radiotherapy group demonstrated a more stable vessel wall than the controls.($P<0.001$). Trends were observed for 'normalizing' effects on vascular diameter and RBC velocity.

Discussion

A restoration of the angiogenic balance was demonstrated by significantly reduced vessel permeability in every treatment group compared to the controls. This gives at least perspective of a reduced interstitial fluid pressure. The largest effects were demonstrated in the cediranib monotherapy group. Furthermore an alleviated hypoxic environment is suggested in the concurrent modality treatment group since normalization effects were seen combined to an increased perfusion. Additionally fractionated radiotherapy did not elicit vascular destruction nor rampant radioinduced angiogenesis, but exerted vascular stabilizing effects. These findings raise incentives on a normalized micro-environment in each treatment group compared to the controls.

SAMENVATTING

Inleiding

Colorectale kanker is de tweede meest dodelijke kanker in Europa. Tumoren ontwikkelen op verschillende manieren betere overlevingskansen en behandelingsresistentie. Aberrante tumor angiogenesis induceert een vijandig tumormilieu waar metastatische tumor cellen kunnen uitgroeien en behandelingsstrategieën niet aanslaan. In preklinische studies heeft cediranib, een krachtige VEGF receptor inhibitor, aangetoond immature bloedvaten te kunnen fnuiken en het tumormilieu te normaliseren. Het wordt verondersteld dat de gecombineerde effecten van cediranib en radiotherapie, afhankelijk van de dosis, ofwel verdere normalisatie uitlokken ofwel vasculaire degeneratie.

Methodologie

Gefractioneerde radiotherapie (1.8Gy dd.) en cediranib (6mg/kg/dag) werden in deze studie ofwel concomitant ofwel als monotherapiën toegediend. De effecten werden geobserveerd via in vivo fluorescentie microscopie door de glaskamertjes op de dorsale huidplooi. Om het klinische doel te behartigen werden menselijke colorectale kankercellen (HT29) geïnjecteerd in naakte muizen. Na drie dagen recuperatie en observatie, werd de behandeling geïnitieerd voor vijf opeenvolgende dagen. 4 behandelingsgroepen werden samengesteld welke ofwel placebo, één modaliteit afzonderlijk of beide modalieteiten tegelijkertijd werden toegediend. De video's werden geanalyseerd door gebruik te maken van videoanalyse software ImageJ of CapImage. Om de normalisatie effecten van de verschillende behandelingsregimes te beoordelen, werden typische tumor vasculatuur variabelen gedefinieerd: het aantal bloedvatvertakkingen, de bloedvat densiteit, diameter, RBC snelheid, debietsnelheid, konkeligheid en permeabiliteit.

Resultaten

Statistisch bewijs voor een reductie in kronkeligheid is aangetoond in de cediranib groep vergeleken met de controle groep. ($P=0.012$). De cediranib groep vertoonde ook de minst permeabele bloedvatwand. ($P<0.001$) Opvallend genoeg vertoonde de radiotherapie groep een meer stabiele bloedvatwand dan de controlegroep. ($P<0.001$). Ook werden trends gezien in de richting van een genormaliseerde diameter en RBC snelheid.

Discussie

Een herstel van de angiogenetische balans is aangetoond door een significant verminderde permeabiliteit voor iedere behandelingsgroep vergeleken met de controle groep. Dit geeft op zijn minst het vermoeden van een verminderde interstitiële vloeistof druk. Het grootste effect is aangetoond voor de cediranib groep. Overigens is als gevolg van de gelijktijdige behandeling van cediranib en radiotherapie een opgeheven hypoxie verondersteld omdat in deze groep naast normalisatie ook een toegenomen perfusie is vastgesteld. Daarenboven heeft gefractioneerde radiotherapie geen radio-angiogenese geïnduceerd, noch bloedvatdestructie, maar eerder een stabiliserend effect op de bloedvaten. Deze besluiten suggereren een genormaliseerd tumor milieu in elke behandelingsgroep vergeleken met de controles.

1. INTRODUCTION

1.1 COLORECTAL CANCER

1.1.1 EPIDEMIOLOGY

Colorectal cancer (CRC) is the third most common cancer in men, it accounts for 13.2% of total cancer incidence, in women it is the second most common cancer with 12.7% of total cancer incidence. In Europe approximately 3.5 million people suffer from any type of cancer and 1.7 million people end up in a terminal stage. CRC is responsible for 12.2% of cancer mortality (equal for men and women), which makes colorectal cancer - only preceded by lung cancer - the second most deadly cancer in Europe. (1)

There is a lifetime probability of 4.7% in women and 5.0% in men for the development of colorectal cancer and a median 5 year survival at diagnosis of 64.9%. (2)

As it comes to health Economics, in the West 10% of cancer-cost is spent on colorectal cancer. Thus there is a strong cue for early detection and treatment. By consequence during an EU council in 2003 the prioritization of early detection was emphasized. (3) A higher cost-effectiveness in the management of cancer lies in better accessibility, sensitivity/specificity and actual cost for a population-based screening program.(4)

1.1.2 ETIOPATHOGENESIS AND MOLECULAR MECHANISMS

95% of colorectal cancers are a result of malignant transformation of sporadic adenomatous polyps. (5) Inherited forms account for 5 to 10% of total CRC prevalence. The two most common types are autosomal dominant inherited: Familial Adenomatous Polyposis (FAP) and Hereditary Non Polyposis Colorectal Cancer (HNPCC).(6)

I SPORADIC COLORECTAL CANCER

The etiopathogenesis of sporadic colorectal cancer commences at aberrant crypt foci in normal intestinal epithelium. These primary lesions are nascent adenomatous polyps. They develop to become metaplastic adenoma's presenting with different levels of dysplasia. 10% shows to turn malignant in 5 to 10 years.(5) The following mechanisms explain the neoplastic transformational process.

II GENOMIC INSTABILITY

The molecular basis of malignant cell proliferation is a combination of genetic and epigenetic abnormalities resulting in genomic instability. This genomic instability results in a dysregulation of natural oncogenic and tumor suppressor functions. The actual tumorigenesis is not a continuous process, it is rather a Darwinian reminiscent process occurring in waves. Each new malignant cell phenotype adopting better growth advantages surpasses the survival of slow ancestor neoplastic cells. The grade of cell dysplasia depends on which types of genetic factors are leading to genomic instability. (7) Specific prognosis determining factors can be molecularly evaluated like KRAS gene and BRAF gene mutations. These mutations make CRC more susceptible to biologic agent therapeutics like cetuximab and panitumumab. (8) Since epigenetic modifications are reversible, ideas for dietary chemoprevention targeting epigenetic modifications seem plausible. (9)

III MOLECULAR BASIS OF CRC

Gene mutations responsible for non-hereditary forms of CRC are caused by oxidative stress. This is a progressive tissue damaging process resulting from the effects of reactive oxidative species (ROS) or reactive nitrogen species (RNS). ROS are mitochondrial produced molecules as a cellular response to changing (stressful) environments. The physiological function of ROS is to enhance subcellular signaling pathways. In hypoxic situations cells switch to the production of RNS. ROS and NOS are normally neutralized by anti-oxidizing enzymes (such as glutathione reductase, catalase, glutathione peroxidase, superoxide dismutase and non-enzymatic anti-oxidants such as glutathione, vit C, vit D). This is schematically presented in figure 1. In sustained environmental stress, an imbalance between oxidants and anti-oxidants is installed. In the presence of oxidant excess, vital structures and functions become oxidatively affected, leading to somatic mutation and neoplastic transformation. (10)

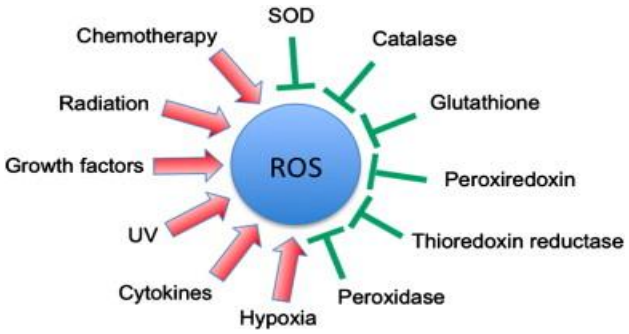

Figure 1: ROS induction as a result of oxidant-anti-oxidant imbalance (10)

1.1.3 RISK FACTORS

The induction of CRC results from complex interactions of multiple risk factors. Typical prominent unmodifiable factors are age, inflammatory bowel disease (IBD) and the presence of inherited phenotypes, illustrated in table 1.

Prominent unmodifiable risk factors of CRC	
Age	More than 90% of CRC-cases are diagnosed over the age of 50. (11)
IBD	In ulcerative colitis (UC), 35 years after diagnosis, there is an absolute CRC risk of 30 percent when presenting with pancolitis, and 40 percent when UC diagnosed at an age of less than 15 years. (12).
Inherited forms	Considering the burden of CRC risk in inherited forms of CRC, FAP accounts for a 100% chance of CRC development at the age of 40. HNPCC encompasses a lifetime risk to develop CRC of 70-80%. (6)

Table 1

I OTHER RISK FACTORS

Relative risk estimates for other relevant modifiable and unmodifiable risk factors contributing to CRC development are stated in table 2 (addendum 1). Also protective factors against CRC development are added. (13)

II GEOGRAPHICAL SETTING

Geographical differences in CRC incidence for men and woman are illustrated in figure 2. (14)Japanese men migrating to the US are exposed to a doubled CRC risk for CRC compared to their fellow native Japanese. (15) Similarly, in an urban-rural setting, urban residents are exposed to a higher CRC risk than people from rural regions. (16)

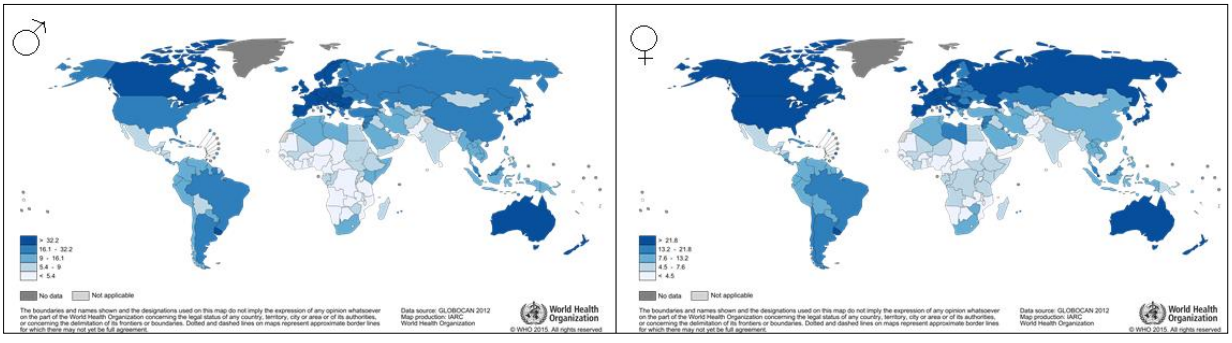

Figure 2: Geographical differences in CRC incidence per gender (14)

1.1.4 PREVENTION

Primary prevention consists of timely resection of colorectal polyposis and modifying environmental risk factors, illustrated in table 3 (addendum 1) (5), and. A retrospective study showed a 53% decrease in CRC mortality by preventive colonoscopic resection of non-adenomatous and adenomatous polyps. (17)

1.1.5 SCREENING

I MASS POPULATION SCREENING

Mass screening for early detection of CRC is performed using fecal occult blood tests (FOBT). Biennial FOBT renders a CRC mortality reduction of 14% when performed over 10 years. Detection of CRC in an early stage renders a survival rate of 95% (18,19) Analyses show excellent cost-effectiveness for FOBT screening programs. (20) In Belgium the instrument of choice for mass screening is the fecal immunochemical test (FIT). Men and women between the ages of 56 and 74 receive a biennial invitation and a sampling set to participate to CRC mass screening. FIT has proven to overrule the benefits of Guaiac FOBT (gFOBT). (19, 21, 22) Additional screening tools to improve detection rates are also included in table 4. (4, 5)

Screening tools for CRC detection	
Screening tool	**Use**
FOBT	Primary screening tool, adopted for mass screening
Total Colonoscopy (TC)	Primary screening tool (60% mortality reduction) or following FOBT as preventive strategy for polyposis deterioration
Sigmoidoscopy	
CT- colonography	Primary screening tool or follow-up in patients refusing TC after FOBT
Stool DNA tests	Experimental, implications for combinational use with FOBT, avoiding excess TC's
Circulating Tumor micro RNA's tests	

Table 4

II HIGH RISK POPULATION SCREENING

In patients that suffer from high risks, such as a first degree relative (FDR) diagnosed with CRC, inflammatory bowel disease, HNPCC and FAP, colonoscopy is the standard tool for primary screening. Screening in this subset of patients starts at a much younger age than in the mass population shown in table 5. (21, 22)

High risk patients and early CRC screening	
FDR	-FDR >60y: colonoscopy starting at the age of 40 with a repetition every 10 years -FDR <60y or more than 1 CRC FDR's: colonoscopy every 5 years starting at the age of 40 or 10 years younger than the age at diagnose of the youngest FDR
HNPCC	Biennial colonoscopy starting at the age of 20-25
FAP	Immediate flexible sigmoidoscopy or colonoscopy and annually repeated until colectomy

Table 5

1.1.6 DIAGNOSIS

I DIAGNOSTIC WORK-UP

The work-up for CRC diagnosis starts with a structured anamnesis followed by a clinical examination. The anamnesis includes the assessment of clinical symptoms and questions about risk factors. An overview of clinical symptoms is stated in table 6. The clinical examination includes the retrieval of a palpable mass in the abdomen and a digital rectal examination. Also blood tests are performed, giving additional information: blood cell count for anemia, liver enzymes for detection of liver metastases and the presence of carcino-embryonic antigen and CA19-9 tumor markers. The latter is usually applied more for progression or recidivist monitoring. (5)

Clinical symptoms of CRC
• **Red blood loss per anum**: directly or after bowel movement, presenting with clear red blood traces in stool or in the toilet. Right-sided CRC accompanied by substantial bleeding shows rather maroon-colored stools as a result of massive hemoglobin oxidation. This is called melena.
• **Abdominal pain**: which is experienced as cramping or discomfort in the lower abdomen
• **Unintentional weight loss**
• **Change in stool**: this can be any change in stool consistence or frequency, for example narrowing of stool shape, diarrhea, constipation...
• **Tenesmus**: the patient experiences an urge to defecate on an empty bowel

Table 6

II STAGING

A colonoscopic biopsy of the malign lesion is preferential to obtain an immediate and accurate confirmation of the CRC diagnosis and its dysplastic gradation. (21, 22) Ultrasonography, CT (chest, abdomen), MRI (liver), liver angiography and PET-scans are crucial to determine the cancer outspread by assessing tumor invasion in nearby tissue, lymph node dissemination and distant metastases. Thus the 'clinical TNM stage' of CRC is determined. TNM stands for Tumor

invasion, Nodal status and Metastasis. TNM staging is used to outline precise treatment policy. (8) Currently the use of the seventh revised edition of AJCC 2010 TNM-classification is encouraged. (23) Figure 3 and 4 show the different TNM stages of colon cancer and rectal cancer respectively.

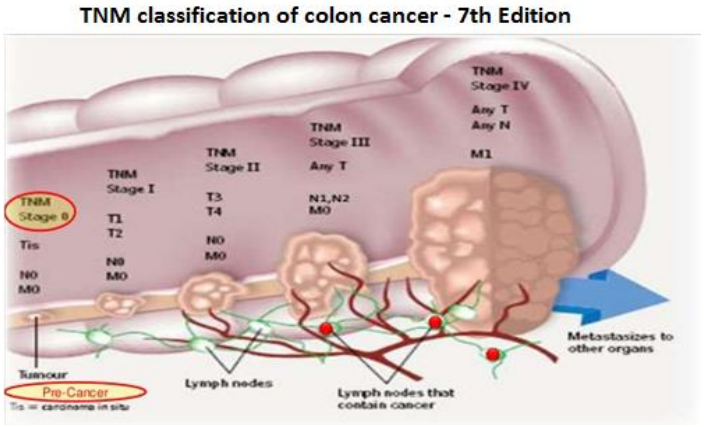

Figure 3: TNM stages for colon cancer 7th edition (5)

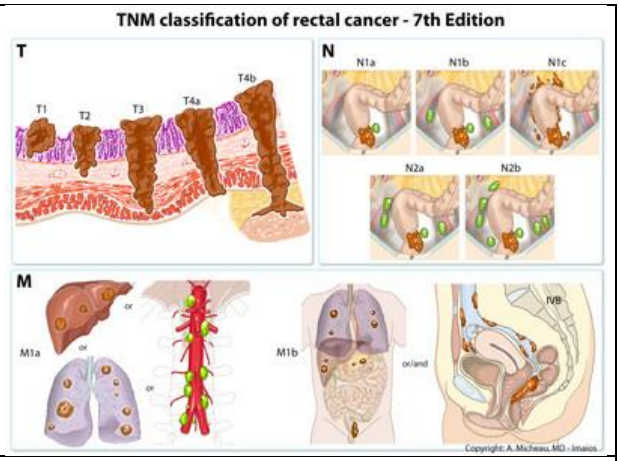

Figure 4: TNM stages for rectal cancer 7th edition (5)

Figure 5 depicts the 5 year survival rates per TNM stage at which colon cancer is diagnosed, adopted from the National Cancer Institute. (24)

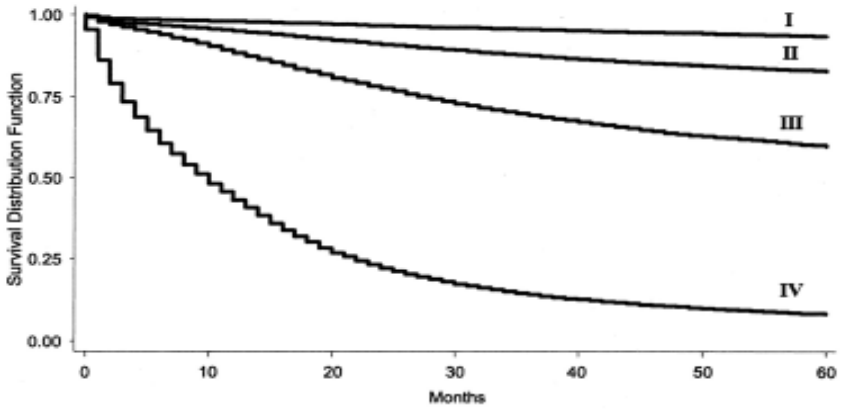

Stage	0 mo		30 mo			60 mo		
	Survival (%)	N	Survival (%)	N	P	Survival (%)	N	P
I	100	14500	96.1	8591	—	93.2	4515	—
II	100	34361	89.2	19492	<.0001	82.5	10105	<.0001
III	100	26949	72.7	12192	<.0001	59.5	5514	<.0001
IV	100	20802	17.3	1832	<.0001	8.1	432	<.0001

Figure 5: 5 year survival rates for colon cancer per TNM stage (24)

After surgery, the specimen is anatomopathologically re-examined to actualize TNM-staging and surgical success. Thus the 'pathologic TNM stage'(pTNM) is determined. Most of the times the pTNM-stage is in concordance with the pre-operative stage. Neoadjuvant therapy could alter the

pTNM. In this scenario, postoperative pathologic staging is designated with an 'yp' prefix (ypTNM). (23)

1.1.7 TREATMENT

Colorectal cancer therapy is adapted to site of origin and TNM-stage. Operative and non-operative modalities are considered.

I OPERATIVE: COLON CANCER

The surgical approach contains invasive procedures, in an attempt to obtain a fully resected carcinoma, with a zero chance of cancer recurrence. The executed procedures according to their respective TNM stages are introduced in table 7.

Operative procedures in colon cancer treatment		
TNM stage	**Anatomical extent of disease**	**Surgical procedure**
0: Carcinoma in situ = Tis	Confined to mucosa (T1) or muscularis propria (T2)	-Simple polypectomy through colonoscopy. -Segmental resection of the colonic wall for larger tumors
I &II: Localized cancer	Penetrates muscularis propria (T3) or invades adjacent organs or structures (T4)	-Tumor resection with additional resection of associated lymph nodes through open laparotomy or laparoscopy (preferable)(25, 26). -High-risk pTNM stage II colon carcinoma with positive tumor budding or tumor border configuration receive additional chemotherapy for six months.
III: Regional cancer	Any tumor stage with lymph node positive characteristics	-Local resection of the whole segment. If the resected specimen shows positive section borders or invasion in adjacent tissues, the procedure is followed by radiation and chemotherapy. -Lymph node positive cancer is post-treated with 6 months chemotherapy. Fluorouracil proves to be effective. -Supplementary adjuvant administration of chemotherapy renders a two years disease free survival bonus.(27)
IV: Distant cancer	Any tumor or nodal stage with invasion of lung, liver, peritoneum or ovary	-Surgery is considered when tumors cause symptomatic blockages or have limited metastases.

Table 7

II OPERATIVE: RECTAL CANCER

Invasive surgical procedures conducted for treatment of rectal cancer differ from treatment of colon cancer. The anatomical sites of tumor spread and external sphincter preservation are important additional keys in determining the excision strategy. Figure 6 shows the anatomical sites of rectal cancer warranting different excision strategies. (28) Table 8 concisely describes the applied techniques. Table 9 outlines the treatment options according to the respective TNM stages of rectal cancer. (5)

Rectal cancer excision strategies		
Total Mesorectal Excision (TME)= coloanal anastomosis	Standard treatment: Tumor is initially prepared and downstaged by neoadjuvant therapy, then resected. -Surrounding tissue is co-prelevated by sharp dissection alongside the avascular visceral mesorectal fascia	-better anatomopathological specimen for stage classification and individualized multidisciplinary treatment consult -rectal cancer recurrence will be less likely (29)
Intersphincteric resection	Tumor invasion is present in the anal ring. This technique is combined with proctectomy and TME (30)	Maintain the normal defecation route despite invasion of the anal ring, which is preferred by most of the patients (31)
Abdominoperineal extirpation	Tumor invasion is present at 2cm or less from the external sphincter or in case of invasion of the levator ani muscle	Results in a colostomy

Table 8

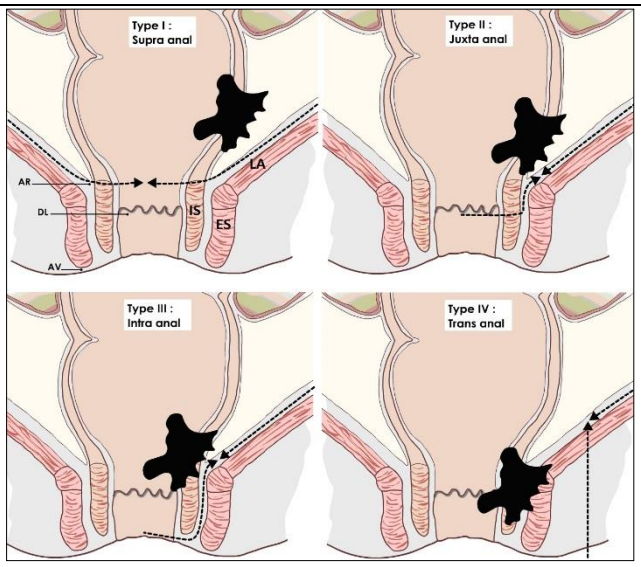

Classification	Definition	Surgical procedure
Type I	Supra-anal tumor > 1 cm from anal ring	CAA
Type II	Juxta-anal tumor < 1 cm from anal ring	pISR
Type III	Intra-anal tumor Internal sphincter invasion	tISR
Type IV	Transanal tumor External sphincter invasion	APR

Type IVa includes the levator ani muscles; IVb, external sphincter; IVc, Levator ani muscles and external sphincter.
CAA = conventional coloanal anastomosis; pISR = partial intersphincteric resection; tISR = total intersphincteric resection; APR = abdominoperineal resection.

AR: anal ring, DL: dentate line, AV: anal verge, IS: internal sphincter, ES: external sphincter, LA: levator ani muscle. Arrowed lines show dissection routes

Figure 6: Anatomical locations of rectal cancer and respective excision strategies

Operative procedure in rectal cancer treatment		
TNM stage	**Anatomical extent of disease**	**Surgical procedure**
0: Carcinoma in situ = Tis	Confined to mucosa (T1) or muscularis propria (T2)	Removed by polypectomy. When a larger size is inspected a segmental resection is performed. This resection may be performed through rectoscopy, thus preventing an abdominal incision (25).
I &II: Localized cancer	Penetrates muscularis (T3) or invades adjacent organs or structures (T4)	Small lesions are still deemed resectable through rectoscopy. Larger lesions require an abdominal approach.
III: Regional cancer	Any tumor stage with lymph node positive characteristics	Treatment options resemble stage I & II. To reduce the chances of cancer recurrence and for treatment of residual positive lymph nodes additional adjuvant therapy is given
IV: Distant cancer	Any tumor or nodal stage with invasion of lung, liver, peritoneum or ovary	Treated analogically to distant stage colon cancer

Table 9

III NON-OPERATIVE MODALITIES

Non-operative procedures encompass radiation and/or chemotherapy and/or biologically targeted therapies. They are most commonly instituted as therapy for distant metastasis. Some subtypes of CRC are specifically susceptible to specialized biological agents which delay, stop or even inverse tumor growth. (5, 32) The standard oncologist treatment regimen for metastasized CRC is FOLFOX or FOLFIRI (5-fluorouracil, leucovorin, oxaliplatin and irinotecan combinations). Recently adjuvant administration of vascular endothelial growth factor (VEGF) and epidermal growth factor receptor (EGFR) biologic pathway inhibitors, such as bevacizumab and cetuximab showed to have potency to improve patient survival. Also aflibercept, a VEGFA-trap molecule has proven its clinical benefit. (33) Although they are commonly used, uniform evidence supporting their effectiveness is missing. Variable response rates are thought to be linked to genetic variability, e.g. differences in KRAS or BRAF mutation.(34) The combined use of non-operative and operative procedures demonstrate beneficial outcomes in preservative strategies. T3 and T4 rectal cancer are firm indications for neoadjuvant chemo-radiotherapy (CRT), eliciting up to 20% pCR (pathologic complete response) rates. (35) Neoadjuvant CRT also has benefits on the resectability of distant staged colorectal cancer. (36)

1.2 MICROVASCULATURE STUDIES

1.2.1 MECHANISMS OF NEOVASCULARIZATION

I NEOVASCULARIZATION MODELS

The formation of new vessels is crucial in embryogenic, wound healing and endometrial physiological processes. Two prominent types of neovascularization are vasculogenesis and angiogenesis. The former relates to the in situ differentiation and proliferation of bone marrow derived hemangioblasts resulting in vessel formation in previously unvascularized regions. The latter relates to maturation, remodeling and expansion of an existing vascular network. Angiogenesis has shown to deploy two distinct mechanisms: vascular sprouting and vascular intussusception. Vascular intussusception generates from the intraluminal ingrowth of an endothelial tissue septum, dividing the existing vessel in separate parts. Hence intussusception is preserved for large vessels. (37, 38) Also in tumors neovascularization is induced. Tumors derive their metabolic supply typically from preexisting vessels by vascular sprouting. (39)

II PHASES OF ANGIOGENESIS BY VASCULAR SPROUTING

The upregulation of VEGFA and VEGF receptor 2 in tumor, stromal and endothelial cells initiate vascular sprouting. The presence of VEGFA in the ECM functions as an angiogenesis guidewire. Furthermore, VEGFA singly enhances the production of its receptor tyrosine kinases (RTK) VEGFR1 and VEGFR2 in endothelial cells (EC), thus inducing increased vascular sprouting. VEGFR2 potentiates endothelial cell mitosis and vessel permeability. VEGFR1 on the other hand mediates the effects of VEGFR2 by sequestrating VEGF from VEGFR2.(40) Physiological angiogenesis by vascular sprouting includes following steps: sprouting, resolution and fusion into a mature vascular bed. In contrast these crucial vascular checkpoints are not achieved by tumorigenic angiogenesis. This is illustrated in table 10 (addendum 1). Figure 7 shows a graphical representation of resolution failure in tumor angiogenesis by constitutionally increased tumor VEGF production and cooptation of immune cells and stromal fibroblasts. The pathways are explained in the following section.

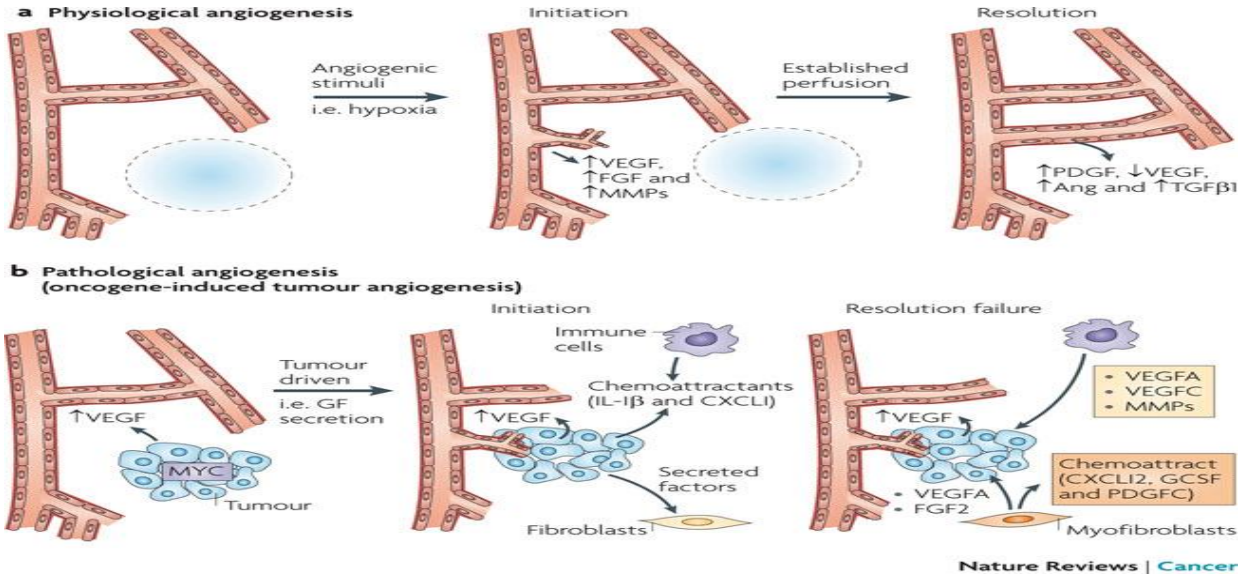

Figure 7: resolution failure in tumorigenic angiogenesis (41)

1.2.2 CRC NEOPLASTIC ANGIOGENESIS CONCEPTS

I TUMORIGENIC ANGIOGENESIS

In tumor microenvironments, several pathways in tumor, stromal, immune and endothelial cells are activated, leading to the expression of proangiogenic factors. This is shown in table 11 (addendum 1). Rapid tumor cell proliferation generates further vascularization and drainage insufficiency. Thus hypoxia and acidosis are installed firing physiological angiogenesis. The end balance is an excess amount of proangiogenic factors outweighing the mediating effects of their anti-angiogenic counterpart.

II ABERRANT MICROVASCULATURE

Hence rampant endothelial cell proliferation and migration, followed by bad pericyte coverage and a defective basement membrane institute, which is considered as defective angiogenesis. Histologically this represents tortuous, saccular and dilated blood vessels with poorly configured and thus hyperpermeable vessel walls. Moreover, as a result of external mechanical pressure from continued cancer cell proliferation, an additional spatially and temporally heterogeneous impaired blood vessel formation institutes. (42)

III INTERSTITIAL FLUID PRESSURE

Since these newly formed vessels lack the ability to maintain physiological transmembrane pressure gradients and no sufficient lymphatic drainage is allowed, an increase in interstitial fluid pressure (IFP) of the tumor ensues, especially in large tumors. (43)

IV SUSTAINED HYPOXIA AND ACIDOSIS

Aberrant tumor blood vessel formation and increased oxygen consumption by proliferating endothelial and tumor cells induce a sustained hypoxic and acidic tumor micro-environment. The hypoxic stress and acidosis lead to further angiogenic triggering and generate repetitive waves of spatially and temporally heterogeneous neovascularization. (42, 44)

1.2.3 INDUCTION OF A HOSTILE MICRO-ENVIRONMENT

The increased IFP, hypoxia and acidosis create a hostile tumor micro-environment which facilitates tumor preselection on invasive cancer cells and metastatic capacity. Thus phenotypic changes to guarantee tumor cell survival are promoted such as increased growth potential and alternative cellular metabolisms. Also badly organized vessel walls admit tumor cells to easily intravasate in the blood circulation, enhancing cancer dissemination.(45) This is also potentiated by increased lymphangiogenesis in the tumor periphery resulting from excess VEGF-C production (46) Furthermore, aberrant microvasculature induces treatment resistance in tumors, as shown in table 12 (addendum 1).

1.2.4 IMAGING TECHNIQUES FOR MICROVASCULATURE

To perform research on architectural and physiological characteristics of tumor microvasculature and the effects of antiangiogenic or antivascular treatment, proper imaging techniques are mandatory. An elegant technique to record dynamic processes in micro-vasculature and micro-environment is intra-vital microscopy (IVM). To optically access the desired area, specific tissue preparation procedures are needed. In 1943 Glen Algire pioneered several techniques for in vivo imaging of mouse models. His dorsal skinfold window chamber (DSWC) technique was a remarkable invention eliciting an important acceleration in angiogenesis research. (47) Although DSWC implantation is associated to perioperative risks and a prolonged recovery time, sufficient optical access remains for 3 to 4 weeks. A proper combinational use of a suitable molecular probe and microscope renders high visibility of molecular targets, high spatial resolution and sufficient optical tissue penetration depth for image acquisition. (46) In table 13 (addendum 1) several microscopes and their respective specifications are shown. A considerate selection of de-noising computer software for image analyses is also recommended. (48) Furthermore to clinically analyze the effects of anti-angiogenic treatment in patients, MRI analyses give good approximations of vascular permeability. (49)

1.3 INTERVENTIONS ON ABERRANT TUMOR MICROVASCULATURE

1.3.1 INTERVENTION GOALS

Goals of anti-angiogenic treatment are lowering the IFP, increasing the global tissue oxygen tension and enabling uniform delivery of metabolites. Perspective is given that by administration of neoadjuvant anti-angiogenesis therapy anti-cancer treatment could be enhanced. Pioneering research on adding anti-angiogenesis treatment to cytotoxic therapy was performed by Teicher et al. in 1998, demonstrating its benefits on treatment efficacy for the first time. (50) Later on in 2005 the hypothesis of a vascular 'normalization window' for cancer treatment was postulated by Jain. (42)

1.3.2 MECHANISM OF ANTI-ANGIOGENIC TREATMENT

Judicious administration of antiangiogenic therapy has shown to restore the angiogenic balance. This is illustrated in figure 8. An introductory presentation of anti-angiogenesis targets is depicted in figure 9. After balance restoration, the tumor microvasculature and microenvironment will not completely regain their normal form, but tend to 'normalize'.(42) During the 'normalization window' oxygen levels rise and IFP levels decrease. Angiogenesis restarts after a certain period, mostly 6 days. In addition Telfer demonstrated that continued anti-VEGF dosing even results in vascular decrease and increased hypoxia.(51) Histologically, during this 'normalization window' immature and leaky tumor vessels are pruned. Also a return of the basement membrane and pericyte coverage is noted. Tumor vessels are deemed to become less dilated and less permeable and the overall tumor-vascular density decreases.

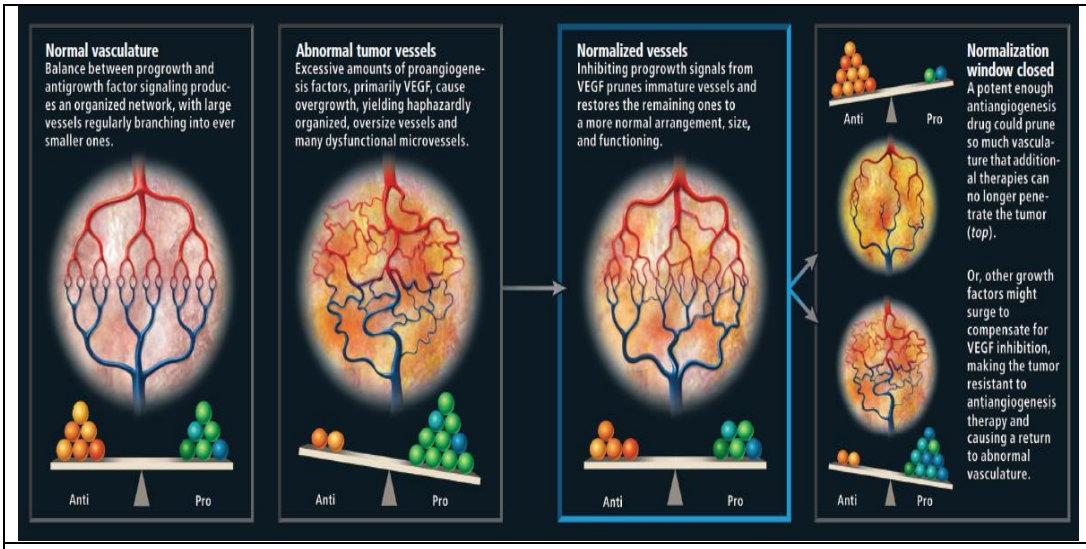

Figure 8: the angiogenic balance and vascular normalization (42)

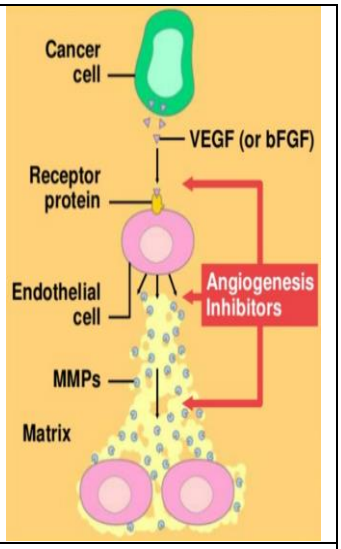

Figure 9: Tumor angiogenesis targets (41)

I CURRENT CLINICAL USE

The concurrent administration of bevacizumab (an anti-VEGFA agent) and chemotherapy gives a survival benefit of 5 months in CRC over chemo alone. Adverse effects of VEGF blockage relate to systems with delicate blood supply like the cardiovascular, endocrine and nervous system. By massively blocking the VEGF cascade the endothelial cell function is disturbed which can lead to arterial thromboembolic events. (42)

1.3.3 DIRECT ANTI-ANGIOGENIC/ANTI-VASCULAR TREATMENT

Since EC, similar to cancer cells, rapidly proliferate, their progression is also halted by the administration of chemo-radiotherapy. Actively targeting the tumor microvasculature can lead to a slight decrease in microvascular and micro-environmental instability and is strongly dose dependent. Direct targeting however shows to be more effective when combined to anti-angiogenic pretreatment. (44)

1.3.4 VEGF INHIBITION COMBINED TO RADIOTHERAPY

Radiotherapy actively targets the tumor microvasculature by intervening on proliferating EC and inducing EC apoptosis (see further). However, to ensure vascular recovery, EC tend to reactively express VEGFR-2. This is called radioinduced angiogenesis. (52) Original fundamental research by Gorski et. al. showed a reduction of the radiotherapeutic vascular destruction by adding VEGF in vitro to human umbilical vein cells, and an induction by adding a VEGF blocker. (53)

The first study on the combined use of radiotherapy and anti-VEGF and the application window chambers was performed by Geng et al in 2001. Since Geng noticed the severity of glioblastoma multiforme to be highly dependent on VEGF expression, he designed a study containing two treatment groups. The first group received anti-VEGF RTK (SU5416) as monotherapy and the second group a combined regimen with anti-VEGF RTK (SU5416) and radiotherapy (2Gy). The former showed only little vascular reduction, the latter showed a large vascular decrease and inhibition of radioinduced angiogenesis. (54)

The association of anti-VEGF to radiotherapy has a temporally ambivalent function: preradiation administration restores the angiogenic balance and increases the oxygen supply, potentiating the ionizing effects of irradiation, according to Winkler et al :

> *"…Here we show that VEGFR2 blockade creates a "normalization window"--a period during which combined radiation therapy gives the best outcome.",* (55)

whereas the anti-VEGF post-radiation effects constitutionally turn off the angiogenic switch leading to unresolved vascular destruction and subsequent tumor starvation. This was postulated by Cao et al:

> *"…When similar combination was applied to the H460 lung cancer xenograft model in nude mice, loss of radiation-induced phosphorylated Flk-1 was observed in the combination treatment group.". (56)*

1.3.4 ANTI-ANGIOGENIC DRUG COCKTAIL

Occasionally, more severe cancers evolve VEGF-independent portions, leading to resistance to VEGF anti-angiogenic therapy. In these cases other molecular pathways (e.g. FGF, BV-8 and IL-8) need to be addressed. Unravelling all of these pathways should lead to the development of the ideal antiangiogenic cocktail. Factors leading to anti-VEGF resistance are the presence of pericyte coverage, myeloid cell recruitment, cancer associated fibroblasts and EC cytogenetic abnormalities.(45) An updated overview of conventional and alternative anti-angiogenic treatment modalities is given in table 14 (addendum 1).(40)

1.4 ANTI-ANGIOGENIC DRUGS: SMALL MOLECULE TYROSINE KINASE RECEPTOR (RTK) INHIBITORS: CEDIRANIB

1.4.1 CEDIRANIB: DRUG PROFILE

Table 15 shows several members of the small tyrosine kinase receptor (RTK) inhibitors family. Cediranib is an orally available selective inhibitor of VEGFR 1,2 and 3 that competes at the ATP-binding location. Cediranib also inhibits stem cell factor (SCF) (c-kit) and the PDGF-β receptor. In vitro, the effects of cediranib were demonstrated by Wedge et al. They discovered a vast in vitro inhibition of proliferating umbilical vein endothelial cells by cediranib administration. Also in an endothelial/fibroblast model they found a manifest reduction of vascular density and branching. Microvascular reducing effects in established tumors were seen at ≥1.5 mg/kg daily by Wedge et al. (57) Figure 10 demonstrates the cediranib binding sites.

Small RTK inhibitors family

INHIBITOR	OTHER NAMES	INHIBITS
Axitinib	AG013736	VEGFR, PDGFR, and c-kit
Canertinib	CI-1033	EGFR, HER2, HER3, and HER4
Cediranib	Recentin, AZD2171	VEGFR, PDGFR-β, and c-kit
Dasatinib	Sprycel, BMS-354825	Abl, Src, and Tec
Erlotinib	Tarceva, OSI-774	EGFR/HER1
Gefitinib	Iressa	EGFR/HER1
Imatinib	Gleevec, STI571	Abl, PDGFR, and c-kit
Lapatinib	Tykerb, GW-572016	EGFR and HER2
Leflunomide	Arava, SU101	PDGFR (EGFR and FGFR)
Motesanib	AMG 706	VEGFR, PDGFR, and c-kit
Neratinib	HKI-272	EGFR and HER2
Nilotinib	Tasigna	Abl, PDGFR, and c-kit
Pazopanib	Armala, GW786034	VEGFR, PDGFR-α and -β, and c-kit
Regorafenib	BAY 73-4506	VEGFR-2 and Tie-2
Semaxinib	SU5416	VEGFR
Sorafenib	Nexavar, BAY 43-9006	Raf, VEGFR-2 and -3, PDGFR-β, and c-kit
Sunitinib	Sutent, SU11248	VEGFR, PDGFR, Flt-3, c-kit, RET, and CSF-1R
Tandutinab	MLN518, CT53518	PDGFR, Flt-3, and c-kit
Toceranib		
Vandetanib	Zactima, ZD6474	VEGFR-2, PDGFR-β, EGFR, and RET
Vatalanib	PTK787	VEGFR, PDGFR-β, and c-kit

VEGFR indicates vascular endothelial growth factor receptor; PDGFR, platelet derived growth factor receptor; EGFR, epidermal growth factor receptor; HER, human epidermal growth factor receptor; FGFR, fibroblast growth factor receptor; CSF-1, colony-stimulating factor-1.
*Please note list is not exhaustive.

Table 15

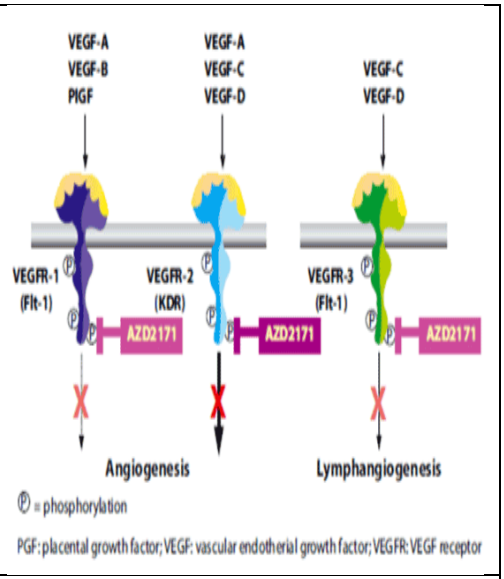

Figure 10: Cediranib binding sites (58)

Other names for cediranib are Recentin or AZD-2171. The primary side effect of cediranib is hypertension, which is often seen in any anti-VEGF cascade treatment due to disruption of the EC function (see above). Fatigue, hand and foot syndrome (peripheral neuropathy), neutropenia, diarrhea, headache, nausea, vomiting, anorexia and weight loss are also common side effects. (59, 60) Less frequent complications are left ventricular dysfunction and hemorrhages. The effective dose range for treatment in in vivo test systems recommended by AstraZeneca is 1.25-

5mg/kg/day. The recommended dose for oncologic use is 30 mg once daily and may depend on risk-benefit considerations.(61). For ovarian cancer the actual drug developmental status of Cediranib resides in the preregistration phase, where safety and curative potency are acknowledged in all phase III studies, but not yet fully approved by the European Medicines Agency for routine practice. (62)

1.4.2 CLINICAL TRIALS ON CEDIRANIB AND METASTATIC COLORECTAL CANCER

Two trials have been conducted to investigate the additional value of the association of cediranib to conventional chemotherapy in metastatic CRC (mCRC). The results are shown in table 16. Although evidence for prolonged progression free survival (PFS) in mCRC is collected, no improvements in overall survival (OS) are seen.(63, 64) Furthermore the HORIZON III trial shows no significant difference in OS and PFS improvements comparing bevacizumab with cediranib for combinational use with chemo in mCRC treatment. (65) These findings are confirmed by Cunningham et al.(66)

Trials on association of cediranib to chemotherapy			
Trial	**Phase**	**Treatment**	**Outcome**
Kato et al; 2012: Japanese double blind RCT, metastatic CRC(64)	Phase II	FOLFOX+cediranib (20mg) vs. placebo + FOLFOX	Hazard ratio for PFS: 0.70; 95% CI, 0.44 to 1.11
Hoff et al; 2012: HORIZON II double blind RCT, metastatic CRC(63)	Phase III	FOLFOX/CAPOX+ cediranib (20mg) vs. placebo + FOLFOX/CAPOX	Hazard ratio for PFS: 0.84; 95% CI, 0.73 to 0.98

Table 16 (FOLFOX =fluorouracil, leucovorin, and oxaliplatin, CAPOX= capecitabine and oxaliplatin)

1.5 RADIOTHERAPY

1.5.1 MECHANISM OF IRRADIATION

Ionizing radiation for cancer treatment generates from the return of heavy atoms from excitation states, thus emitting an energy load under the form of α, β and γ subatomic particles or high frequency spectrum electromagnetic waves. When the ionizing radiation is directed at a specific tissue area, the transduction of energy leads to an increase in the excitation states of tissue molecules with subsequent release of electrons from their orbits. In this manner the affected atoms become oxidized. Specifically the oxidization of O2 molecules is of importance because of their ubiquitous presence and free movement. The oxidized O2 molecules become free radicals, these are reactive oxidative species (ROS) and have the potency to ionize and destabilize lots of organic structures, such as DNA.

Irradiation also generates an ion from [$H2O + \gamma \rightarrow H2O^{+} + e-$]. Several interactions of this ion to other water molecules lead to the production of two supplementary ROS: hydronium ions and hydroxyl radicals [$H\ 2\ O^{+} + H\ 2\ O \rightarrow H\ 3\ O + OH\bullet$]. Hydroxyl radicals inflict severe DNA damage by DNA single strand breaks (SSBs), double-strand breaks (DSBs), base pair damage or cross-link damage. Damaged DNA leads to cell apoptosis. This mechanism is naturally intervened by an enzyme, poly-ADP-ribosepolymerase (PARP), assisting in base excision repair (BER) of SSBs. (51)

Since inert structures do not experience any function loss by ionization they remain unaffected. Quick proliferative processes that depend on delicate molecular regulation are much more affected. Hence stromal and angiogenic processes and cancer growth are halted by radiotherapy. These different processes were shown to influence each other (67).

1.5.2 FRACTIONATED RADIOTHERAPY AND VASCULAR MODULATION

It is presumed that carefully fractionated radiotherapy in low doses can lead to certain angiogenic balance restoration and increased perfusion. (68-72) In treatment regimens, the vascular status in response to radiotherapy is initially unaffected, if not improved, but degenerates as further radiotherapy is administered. In xenograft tumor models the application of 5 to 10Gy dd shows little vascular modulation, but increasing the radiation dose beyond 10 Gy induces severe vascular damage.(73)

1.6 CEDIRANIB COMBINED TO RADIOTHERAPY

The theoretical basis is outlined earlier. Table 17 illustrates recent research on the combined use of cediranib and radiotherapy in human xenograft mouse models. (56, 74-76) Chronic combined treatment (cediranib prior to each radiotherapy session and daily thereafter) and sequential combined treatment (cediranib following each radiotherapy session) have shown equally to decrease vascular density and total perfusion and to increase tumor growth inhibition more than treatment with each modality alone. (56, 74-76)

Research on combined cediranib and radiotherapy in mouse xenograft models			
Study	**Cancer type**	**Modalities**	**Effects**
Wiliams KJ et al; 2008 (74) (No DSWC)	Lung: Calu-6 tumor cell line	Concurrent cediranib (3mg/kg, 5days) and radiotherapy (2Gy, 5 days)	Enhanced tumor growth inhibition, anti-vascular effects and increased hypoxia
Bozec A et al; 2007(76) (No DSWC)	Head and neck: Cal 33 tumor cell line (highly EFGR expression dependent)	Concurrent cediranib (2.5mg/kg, 5days/week) and radiotherapy (6Gy 3 days/week) for 2 weeks, also association of EGFR-inhibitor was tested	Enhanced tumor growth inhibition, and reduced EC activity
Wiliams KJ et al; 2007(75)	Lung: Calu-6 tumor cell line Colon: LoVo tumor cell line	Concurrent cediranib (3mg/kg, 3days) and radiotherapy (5-10Gy, 3 days) 3 times daily	Qualitative changes: less vessel branching, smoother appearance, vessels disappearing
Cao C et al; 2006(56) (No DSWC)	Lung: H460 tumor cell line	Concurrent cediranib (0.75mg/kg, 7days) and radiotherapy (2Gy, 5 days)	Enhanced tumor growth inhibition, large decrease In vascular density, higher apoptosis rates

Table 17

1.7 AIM

The aim of this study is to investigate the effects of cediranib and radiotherapy on micro-vessel structure and function in human colorectal cancer xenograft mouse models using in vivo microscopy in DSWC. By defining a set of microvascular variables, data were acquired for statistical analyses to quantitatively objectify in vivo vascular normalization effects.

2. MATERIAL AND METHODS

2.1 CANCER CELL LINE AND ANIMAL MODELS

2.1.1 CELL LINE

The HT29 cell line, a human colon carcinoma cell line, provided by the by the Department of Experimental Cancer Research, Ghent University, Belgium, was used for this study. A suspension of $1x10^6$ HT29 cells in 20µL Matrigel was injected in the dorsal skinfold window chamber at day 0.

2.1.2 ANIMALS

Animal experiments were approved by the Animal Ethical Committee of the Ghent University, Belgium. Foxn1nu male mice (ENVIGO, The Netherlands) of 8 weeks old were used, as they show excellent compatibility to support xenograft HT29 colorectal cell growth. Animal care throughout the experiment was provided by certified professionals. The animals were held separately in plastic cages with free access to tap water and standard pellet food. At the end of the experiment (8 days after tumor cell injection), mice were euthanatized by cervical dislocation.

2.2 EXPERIMENTAL THERAPY

Treatment was started at day 3 after tumor induction and given for 5 consecutive days. There were 4 treatment groups, with 6 to 8 animals in each group. The first group consisted of controls, the second group was treated with cediranib monotherapy, the third group received radiotherapy, and the fourth group was subjected to concurrent treatment of cediranib and radiotherapy. Radiotherapy was administered with the Small Animal Radiation Research Platform (SARRP), after mice were anesthetized. The anesthesia regimen consisted of inhalation of sevoflurane (flow: 1 -1,5L/min) dosed at 8% for induction and 4 to 5% for maintenance. Cediranib (Astra Zeneca, Brussels, Belgium) was dissolved in a 1% polysorbate 80 (tween 80) solution of deionised water which was sterilised by autoclaving . Treatment protocols are outlined in table 18.

Material and Methods: Treatment protocols	
Treatment Groups	**Day 3 to 7**
Group 1:	Vehicle: 15µl of 1% polysorbate 80 (10g deluted in 1l destiled water), oral gavage 1x dd
Group 2:	Cediranib: 6mg/kg, oral gavage 1x dd
Group 3:	Radiotherapy (RT), 1,8 Gy 1x dd, under anesthesia
Group 4:	Cediranib + RT: 6mg/kg, oral gavage 1x dd (2h pre-RT) and RT under anesthesia, 1,8 Gy 1x dd

Table 18

2.3 DSWC IMPLANTATION

The tumor microvasculature and microenvironment were visualized using the dorsal skinfold window chamber technique. Figure 11 shows an optical window chamber immediately after implantation.

2.3.1 IMPLANTATION TECHNIQUE

Under general anesthesia (Isoflurane, 5% induction, 1.5% maintenance) and analgesia (Ketoprofen, 5mg/kg), mice were positioned on a heating pad to implant the DSWC. The posterior part of the titanium chamber was fixed with sutures (PDS 6-0) to a skinfold on the midline of the back. Next, a circular skin flap was unilaterally excised (dermis and subcutis according to figure 12), giving optical access to the microvasculature of the opposing fascia, whilst adequately humidifying the chamber with saline water. Then, the anterior part of the chamber was attached, fixed with screws and closed with a cover glass. After implantation, mice were placed separately in cages to recover and undergo regular inspection on thrombosis, bubbles, inflammation and infection. A DSWC-implanted mouse is shown in figure 13. The detailed protocol is added in addendum 2.

2.4 INTRAVITAL MICROSCOPY

Imaging was performed through intra-vital fluorescence microscopy on day 0 and day 8 after tumor induction. Mice were anesthetized with sevoflurane and transferred to the pre-heated microscope stage. With a modified Olympus BX50W, fluoroscopic 10x magnified images were made after administration of 0,03ml FITC-D (Fluorescein isothiocyanate–dextran, MW 40kDa) dissolved in NaCl 0.9% (20mg/mL) into the tail vein of the mouse. Static and dynamic images were generated with a HBO 50W mercury lamp and a fluorescein isothiocyanate filter set

(excitation filter 460–490 nm). Due to its minuscule size the FITC-D diffuses rapidly from the intravascular compartment to the extravascular. Hence both intravascular and extravascular epifluorescence are detected. Images were captured by a digital camera and transferred to a computer hard disk. More details about the imaging procedure are depicted in table 19.

<table>
<tr><th colspan="6">Video microscopy time sets</th></tr>
<tr><th>In-tumor location</th><th colspan="4">Image registration time (0''= FITC-D injection)</th><th colspan="2">Measurements</th></tr>
<tr><td>Central</td><td>0''-30''</td><td>1'30''-2'00''</td><td>4'30''-5'00''</td><td>15'00''15'30''</td><td>Permeability</td><td rowspan="3">Vascular Branching, Density, Diameter, Red blood cell velocity and Volumetric blood flow, Tortuosity</td></tr>
<tr><td>Right upper quadrant</td><td colspan="4" rowspan="2">After 15'30''</td><td rowspan="2"></td></tr>
<tr><td>Left lower quadrant</td></tr>
</table>

Table 19

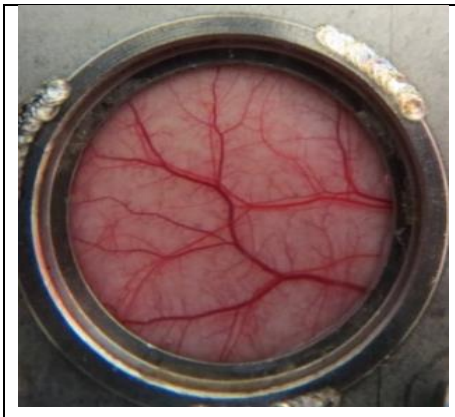

Figure 11: optical window chamber

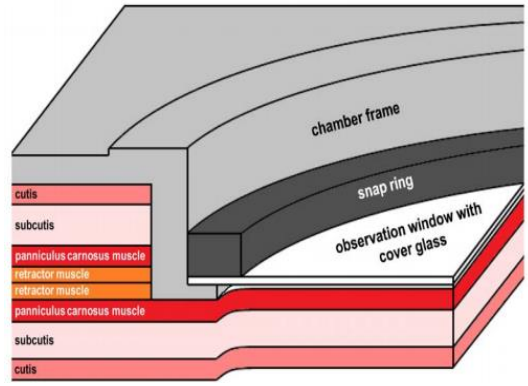

Figure 12: DSWC tissue preparation (77)

Figure 13: DSWC implanted mouse (78)

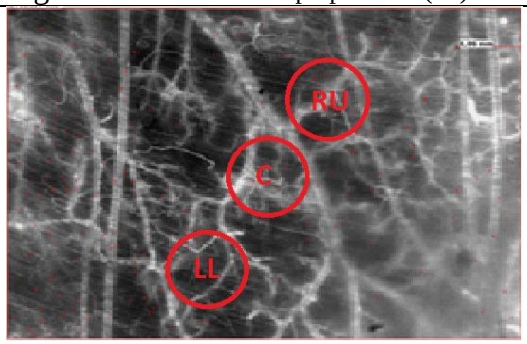

Figure 14: Image analyses areas of interest

2.5 DATA ACQUISITION

2.5.1 CAPIMAGE

Data were calculated by quantitative off-line videometry. Time set specifications according to variable properties are shown in table 19. The definition of each variable is described in table 20. CapImage (H Zeintl Engineering, Heidelberg, Germany) was used for measurements of vascular branching, density, diameter, red blood cell velocity and volumetric blood flow according to Lashke et al. (79) These variables were measured in the central (C), right upper (RU) and left lower (LL) tumor area. This is shown in figure 14 on a 4x zoom image.

I N/A (=NUMBER/AREA)

To analyze the microvascular branching changes, countings of each and every vessel branch were used as variable data. For each mouse, the ratio of mean vascular number of day 8 over day 0 was calculated and used for statistical analyses. 138 videos were selected. Inclusion criteria were a clear vision on blood vessels and one representative video for each tumor area in the DSWC. 8 videos were excluded from the cediranib group because of gross edema and 2 additional videos were excluded from the radiotherapy group because of manifest debris, leaving 128 useable videos.

II L/A (=LENGTH/AREA)

Measurements of vascular density were made through drawings along each visible vessel on the microscopic image. CapImage calculated the total vessel density according to these drawn lines and adapted the measurements to the scale settings. Ratios of mean vascular length of day 8 over day 0 were calculated. Inclusion criteria were a sufficient blood vessel visibility and one representative video for each tumor area. The same videos were excluded as in vascular branching analyses. To calculate a reliable vascular density on each video no coverages by edema or necrosis were desired. In conclusion 128 videos were used for density analysis.

III DIAMETER

Data acquisition for the microvascular diameter was performed through the random assignment of 10 vessels that cross an imaginary line running through the exact middle of the video according to Laschke et al (79). In each vessel a diameter line was drawn and CapImage subsequently calculated the diameter in adaption to the scale settings. Ratios of mean diameter of day 8 over day 0 were calculated for each mouse to quantify the change in micro-vessel diameter.

Inclusion criteria were a clear video and a representative video for each tumor area. Since data acquisition for microvascular diameter only required certain vessels, a smaller chance of compromising analyses by interference of edema of necrosis was expected. Consequently no exclusions were performed and 138 videos were recruited for analyzing.

IV RED BLOOD CELL VELOCITY

To measure the velocity of red blood cells, 10 blood vessels were randomly selected across an imaginary line running through the exact middle of the image according to Laschke et al (79). A line was drawn perpendicularly across each vessel lumen to measure the amount of contrast flowing through at each time. Then, CapImage calculated the red blood cell velocity. The ratio of mean velocity of day 8 over day 0 was calculated in MS Excell. It has to be taken into account that the exact same locations of the microvascular diameter measurements have to be used to allow for the volumetric blood flow formula to make sense. Video inclusion criteria were a clear image and one representative video for each tumor area. Following the same arguments to composite the microvascular diameter sample, 138 videos were selected.

V VOLUMETRIC BLOOD FLOW

An attempt to approximate and simulate blood vessel perfusion was delivered by calculating the volumetric blood flow. This resulted from a formula involving the red blood cell velocity and vascular diameter, see formula 1 (79, 80). Ratios for mean volumetric blood flow of day 8 over day 0 were calculated. Criteria for inclusion were applicability of paired data for transformation according to formula 1 in MS Excell. No data were excluded, giving a selection of 276 data.

2.5.2 IMAGEJ

Vascular permeability and tortuosity were calculated with ImageJ (NIH ImageJ software, Version 1.48).

I TORTUOSITY

The tortuosity index represents the type of endothelial cell migration through the extra-cellular matrix. In tumor tissue this occurs in a non-linear way due to angiogenic imbalance. Tortuosity was calculated according to Norby et al, with the following formula: T (%)= (1-SP/L)*100, where SP represents the shortest distance between 2 branching points (i.e. the distance between two branching points along a straight line) and L represents the segment length (i.e. the distance between the branching points along the vessel). This was expressed as a percentage. (81) 10

vessels crossing an imaginary line in the exact middle of the image were randomly selected. The ratios of mean tortuosity of day 8 over day 0 were calculated and presented as mean tortuosity index for each treatment group. Inclusion criteria were a clear microscopic image and one video representative for each tumor region. Since only 10 vessels were needed per video, no exclusions were done on grounds of insufficient qualitative vessel recruitment. 138 videos were selected for data acquisition.

II PERMEABILITY

The permeability index is a variable measuring the velocity of contrast extravasation over a specific time window, thus representing the vascular leakiness. 10 areas in the interstitium at day 8 were assigned in ImageJ per video and serially measured for contrast intensity. (82)The ImageJ TimeSeriesAnalyzer plugin registers contrast intensity on each video frame (total 552 per video) and on the exact same location at 0', 1'30, 4'30 and 15' of in vivo microscopy. Data of the first 30" were then transferred to Graphpad, where the permeability indices were calculated as coefficients of non-linear regression equations. (49) Parameters acquired from the other registration time points were calculated in SPSS. 138 videos were included for data acquisition. Since only 10 demarcated areas were required for intensity registration no videos were excluded on grounds of tumor overgrowth, edema or radionecrosis.

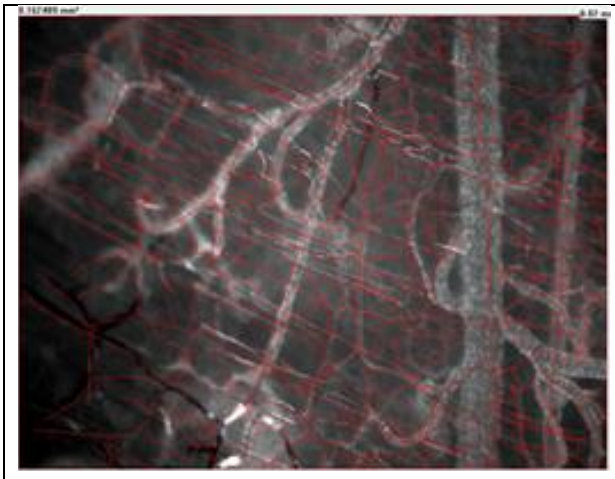

Figure 15 Vascular density videometry

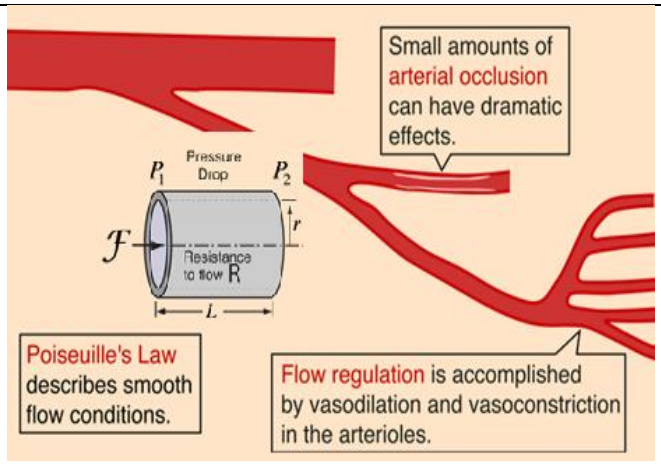

Figure 16 Poiseuille's law for volumetric flow

Variable definitions	
Variable	**Definition**
Number per area (N/A)	Ratio for the mean amount of blood vessel branches per microscopic field of day 8 over day 0, this is further called the vascular branching (81) (78)
Length per area (L/A)	Ratio for the mean length of blood vessel branches per microscopic field of day 8 over day 0, shown in figure 15, this is further called the vascular density. (79, 81)
Diameter (D)	Ratio for the mean blood vessel diameter per microscopic field increase of day 8 over day 0 (79)
Red Blood cell Velocity (RBV)	Ratio for the mean Red Blood Cell velocity per microscopic field of day 8 over day 0 (79)
Volumetric Blood Flow (VQ)	A mathematical variable (80): Ratio for the mean blood vessel perfusion capacity of day 8 over day 0 according to an adaptation of Poiseulle's law where perfusion is related to RBV-profiles and tube diameter. This is illustrated in figure 16 and formula 1 (79)
Tortuosity (Tor)	Ratio for mean index of blood vessel deviation from a linear standard of day 8 over day 0 (83)
Permeability (Per)	Mean index for FITC-D contrast extravasation over time at Day 8 (49, 82)

Table 20

$$VQ = \pi \left(\frac{D}{2}\right)^2 * \frac{V}{K}$$

Formula 1 (K = Baker and Wayland factor= 1.30)

2.6 STATISTICAL OPERATIONS

SPSS statistical package (IBM Corp., version 23, New York, United States), SigmaPlot (Systat Software, version 13, San Jose, United States)) and Graphpad (GraphPad Software, Inc., California, United States) were used for statistical operations. To calculate intergroup differences, the ratios of changes in microvascular structure and function were compared in univariate statistical tests. Descriptive statistics and normality tests were performed in SPSS. Since very little sample sizes are designed, data often pass normality tests due to lack of power. Hence positive Shapiro-Wilk tests (indicating a Gaussian distribution) are ignored. (84) Inductive statistics were performed in SigmaPlot and Graphpad. To calculate significant inter-group differences the following tests were used: one-way ANOVA for parametric distributions in SigmaPlot, one-way ANOVA on ranks for non-parametric distributions in SigmaPlot and non-

linear regression analysis in Graphpad. The zero hypothesis of no significant difference was rejected at less than ≤5% significance level (α). Box-and-whisker plots were designed in SPSS. Post-hoc analyses were done in SigmaPlot using the student's T test for parametrical distributions and the Mann-Whitney U rank sum test for non-parametrical distributions. Each described variable in the above was statistically analyzed.

3. RESULTS

3.1 SAMPLE SIZE

Data were acquired from in vivo microscopy video analyses. To perform meaningful quantitative measurements, the image quality needed to correspond to certain standards. In total 464 in vivo videos were made. Criteria for performant video analyzing were a clear image and sufficient contrast perfusion. Other specifications were often required for some variables. Of the 464 videos, 128 were excluded on grounds of a compromised tumor induction method. In this subset, which was the first pilot, HT29 cells were grown on donor mice, transplanted in dorsal skinfold window chambers of acceptor mice and subsequently analyzed. These analyses showed no reliability since many of these transplanted grafts showed high inflammation rates, impairing the required quality standards. 336 microscopic videos were taken from tumors induced by direct subcutaneous injection of HT29 in acceptor mice. These images rendered better quality. 48 images from the injected tumor group were additionally excluded because no adequate in vivo microscopy could be performed. Main causes for inadequate in vivo microscopy were overstretched skinfolds, bleeding, air bubbles or inflammation.

3.2 RESULTS PREVIEW

Before quantitative analysis, general considerations and variable outcome presumptions were formulated. Table 21 shows representative images for each treatment group. The left column shows images taken at day 0, the right column shows images taken at day 8. Each row has a code. Row 1 relates to the control group, row 2 the cediranib treatment group, row 3 the radiotherapy treatment group and row 4 the concurrent radiotherapy and cediranib treatment group. The red lines drawn across the image indicate the course of the vessels, enlightening their presence. These red lines were used for length analyses (see earlier). It is useful to hold the microscopic images page at hand to visualize the following discussion on qualitative tumor microvascular changes.

Imaging of each treatment group

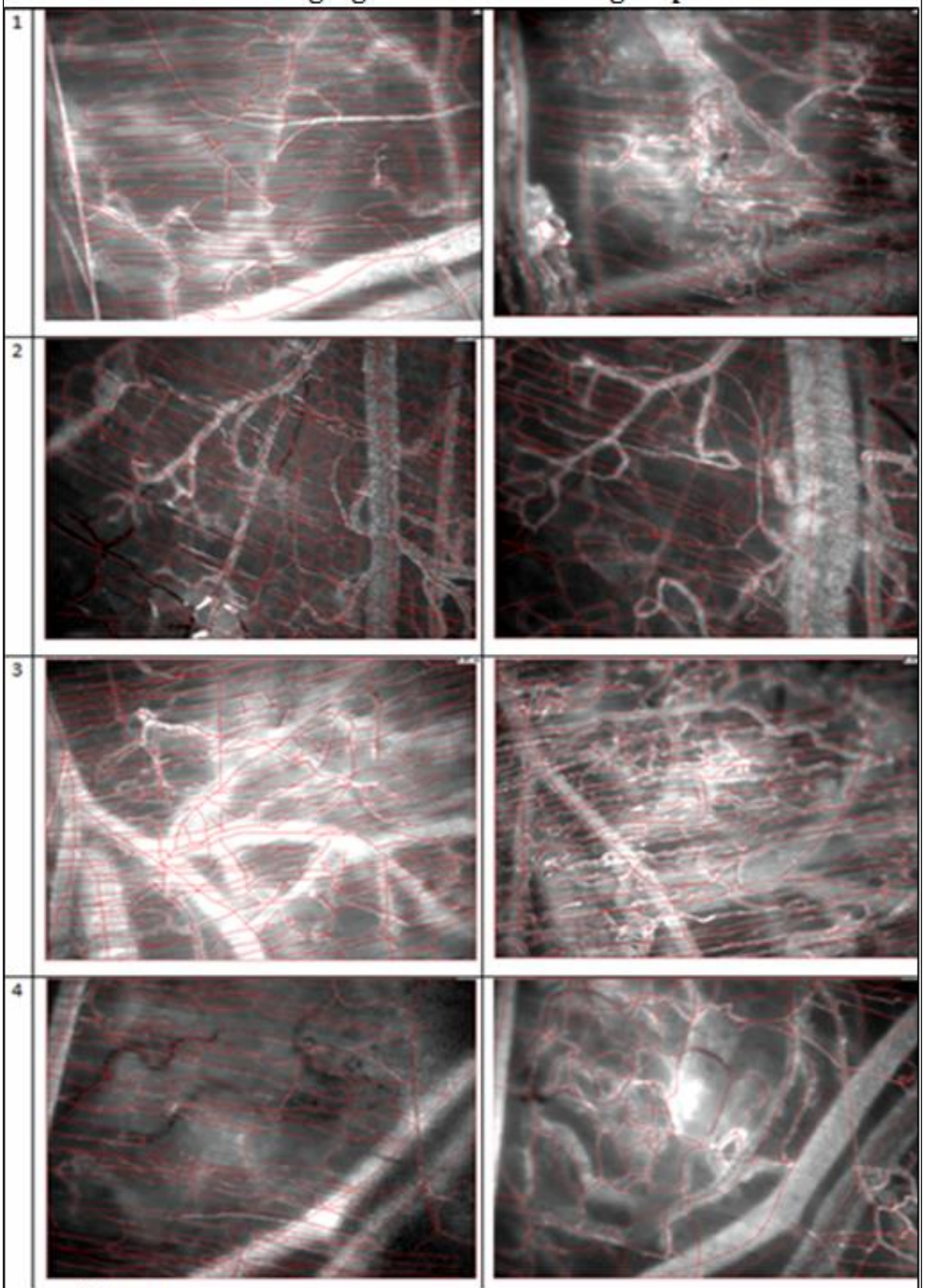

Table 21

3.2.1 Controls group

An overall view on vascular changes in the control group predicted an increase in vascular branching and density following new vessel formation. Also an increase in vessel diameter due to endothelial cell instability, lacking pericyte coverage and basement membrane was hypothesized. An increased tortuosity following improper vessel wall formation and EC migration were presumed. The centerline red blood cell velocity was observed to be decreased. Regarding the vessel wall permeability, a look at the 15' videos predicted an large increase in leaked contrast. Nevertheless, tumor overgrowth made it hard to scan blood vessel properties, rendering some images non-analyzable.

3.2.2 Cediranib treatment group

In the cediranib group a slightly augmented vessel branching and density were seen. Tumor blood vessels did not seem to have gained tortuosity at day 8. Interestingly, blood vessels at day 8 showed less dilatation and were very well perfused. Furthermore, a relatively low permeability gradient was examined. In some images, quality standards were lost due to edema.

3.2.3 Radiotherapy treatment group

In the radiotherapy group, images showed a slight decrease in vascular branching and density. Remarkably, more often the small blood vessels were affected and disappeared. Also some vessels were observed not to be perfused. This could be explained by complete vessel wall destruction. Blood vessel diameters appeared to have increased at day 8. Centerline RBV and VQ seemed to be decreased. In table 21 the picture however demonstrates a contradictory large increase in branching and density. Though, this picture is selected for its clear visibility and is still representative since the increase is explained by radio-induced angiogenesis as mentioned in the introduction. The neovascularization vessels in the picture are very tortuous and permeable, reminiscent of the angiogenesis in the control group. In the radiotherapy group select images were not appropriate for data acquisition of some variables. Image quality in these cases was impaired by the generation of irradiation debris.

3.2.4 Concurrent radiotherapy and cediranib treatment group

In this treatment group, an overall examination of microvascular properties learned that the vascular branching and density were decreased. Again small vessels seemed to have disappeared from the image following irradiation destruction. Larger vessels showed a remarkably increased

perfusion and dilated diameters. Their permeability was not elevated. A slight increase in tortuosity was seen, vessels also showed to be more meandering than tortuous. Possibly the vessel wall formation was more adequate and endothelial cell migration was more organized. Less to no neovascularization was seen compared to the radiotherapy group.In some images, data acquisition was compromised by an edematous blur. However, this was less disturbing than in the cediranib monotherapy group.

3.3 VARIABLE ANALYSES

To deliver statistical significance to the abovementioned notifications, certain variables, which were defined in the material and methods section, were analyzed. The graph page is included after the statistical analyses section.

3.3.1 MICROVASCULAR BRANCHING

In addendum 3 descriptive statistics for the microvascular branching data were added. A box-and-whiskers plot is shown graph 1. The data in each group showed a Gaussian distribution, this was however ignored. (addendum 3). A one-way anova test on ranks was executed in Sigmapot to examine significant intergroup differences (addendum 3). This test showed no statistical significance (P = 0,456). Though a meaningful analysis for vascular branching was deemed to be performed. Since micro-vessels in the concurrent modality treatment group were destroyed and no neovascularization was allowed, a Mann-Whitney U test should have shown significant difference to the controls group. The Mann-Whitney U test was not significant in Sigmaplot (P = 0,937).

3.3.2 MICROVASCULAR DENSITY

Descriptive statistics in SPSS were added to addendum 3. In graph 2 a box-and-whiskers plot is shown. The data in each treatment group were normally distributed, this was however ignored (addendum 3). To measure a significant intergroup difference, a one-way ANOVA test on ranks was executed in Sigma (addendum 3). The intergroup difference was significant (P = 0,039). Decreased density ratios were seen in the cediranib and especially in the controls group which were very unlikely to be true. Also a very low ratio was observed for the radiotherapy group. The concurrent modality treatment group was expected to have a decreased ratio. A significant

difference was demonstrated between the concurrent modality treatment group and the radiotherapy monotherapy group, this was however very unlikely. (P=0.033) (addendum 3)

3.3.3 Microvascular diameter

Descriptive statistics in SPSS were added in addendum 3. In graph 3 a box-and-whiskers plot is included. The data for microvascular diameter showed a normal distribution, this was however ignored. (addendum 3) To statistically demonstrate significant intergroup difference, a one-way ANOVA test on ranks was performed in Sigma. No significant difference could be evinced (P = 0,355). The significant difference between the cediranib monotherapy treatment group and the controls group was examined by a Mann-Whitney U test in Sigma. The Mann-Whitney U test showed no significant difference (P = 0.240). Significant difference between the concurrent modality treatment group and the controls was tested with a Mann-Whitney U test. This showed no statistical significance (P = 0,180).

3.3.4 Centerline red blood cell velocity

Descriptive statistics were added in addendum 3 . Graph 4 shows a box-and-whiskers plot for red blood cell velocity data. The data for centerline RBC velocity were normally distributed, this was however ignored. (addendum 3) A one-way ANOVA test on ranks was performed in Sigma to prove significant intergroup difference. No statistical significance was demonstrated (P = 0,785). To determine whether the cediranib group showed less stasis than the controls group a Mann-Whitney U test was performed in Sigma. The test showed no significance (P = 0,699) Since red blood cell velocity was impaired by instable vessel wall conductance, increased amount of bifurcations, external mechanical pressure from tumor growth and vessel leakiness (Fukumura 2010), a Mann-Whitney U test should have demonstrated significant difference between the concurrent modality treatment group and the controls group. The Mann-Whitney U test was not significant. (P = 0,394)

3.3.5 Volumetric Blood Flow

The descriptive statistics were added in addendum 3. A box-and-whiskers plot is included in graph 5. The data for volumetric blood flow were not normally distributed. A globally increased volumetric blood flow was noted. A one-way ANOVA on ranks test was run in Sigma to examine significant intergroup difference. No significant intergroup difference was demonstrated (P = 0,625). A Mann-Whitney U test was performed in Sigma to demonstrate statistical significance

between the cediranib monotherapy group and the concurrent modality treatment group. No significance was proven by the Mann-Whitney U test (P=0.937).

3.3.6 TORTUOSITY INDEX

Descriptive statistics in SPSS were added in addendum 3. A box-and-whiskers plot is shown in graph 6. The tortuosity index ratios were not normally distributed. To demonstrate significant intergroup differences, a one-way ANOVA on ranks test was run in Sigma. The one-way ANOVA on ranks test showed a significant intergroup difference in tortuosity index ratios (P=0.012). The Mann-Whitney U test was performed in Sigma to prove statistical significance between the controls group and the cediranib monotherapy group. The Mann-Whitney Utest showed a statistical significant difference (P=0.002). A Mann-Whitney U test was performed to examine significant difference between the radiotherapy monotherapy group and the concurrent modality treatment group (addendum 3). The Mann-Whitney U test showed no significant difference (P = 0,937). A Mann-Whitney U test was performed between the controls group and the concurrent modality treatment group in Sigma. The Mann-Whitney U test was not significant (P = 0,456).

3.3.7 PERMEABILITY INDEX

Descriptive statistics by means of non-linear determination coefficients (R^2), rate constants (K, which stands for slope and decay of the curve), spans and plateaus (which stand for the start and end point of the curve respectively) were performed in Graphpad and included in addendum 3. Other descriptive statistics for 1’30’’-2’00’’ and 15’00’’-15’30’’ registrations of day 8 were performed in SPSS and also added to addendum 3. Both were not normally distributed. In graph 7 the changes in extravasation per treatment group were clearly illustrated. Different behaviors were seen in the first 0’30’’, the peak diffusion 1’30”-2’00” and resolution 15’00-15’30’’ time registrations.

I 0’00’’-0’30’’

The F test determined the difference in increase in degrees of freedom using the one-curve-fits-all model against different curves separately in Graphpad. The difference was shown to be statistically significant (P<0.001). A manually performed student’s T test between the regression plateaus of the cediranib monotherapy group and the concurrent modality treatment group in the first 30’’ of day 8 showed a statistically significant difference (two-tailed P<0.001) A manually

performed student's T test between the controls group and the cediranib monotherapy group regression plateaus in the first 30'' of day 8 was significant (two-tailed P<0.001) A manually performed student's T test between the regression plateaus of the controls group to the concurrent modality treatment group in the first 30'' of day 8 was significant (two-tailed P value P<0.001). The residuals to these plateaus however were not normally distributed.

II 1'30''-2'00''

A Man-Whitney u rank sum test was performed between the controls group and the radiotherapy monotherapy group at 1'30"-2'00" of day 8 in Sigma. A significant difference was demonstrated (P<0.001).

III 15'00''-15'30''

A Man-Whitney U Rank Sum test in Sigma between the cediranib monotherapy group and the concurrent modality treatment group at 15'00'' was performed (P<0.001). A Mann-Whitney U test comparing the effects of concurrent modality treatment to the controls group at 15'00" of day 8 was performed. The Mann-Whitney U test showed a significant difference. (P<0.001).

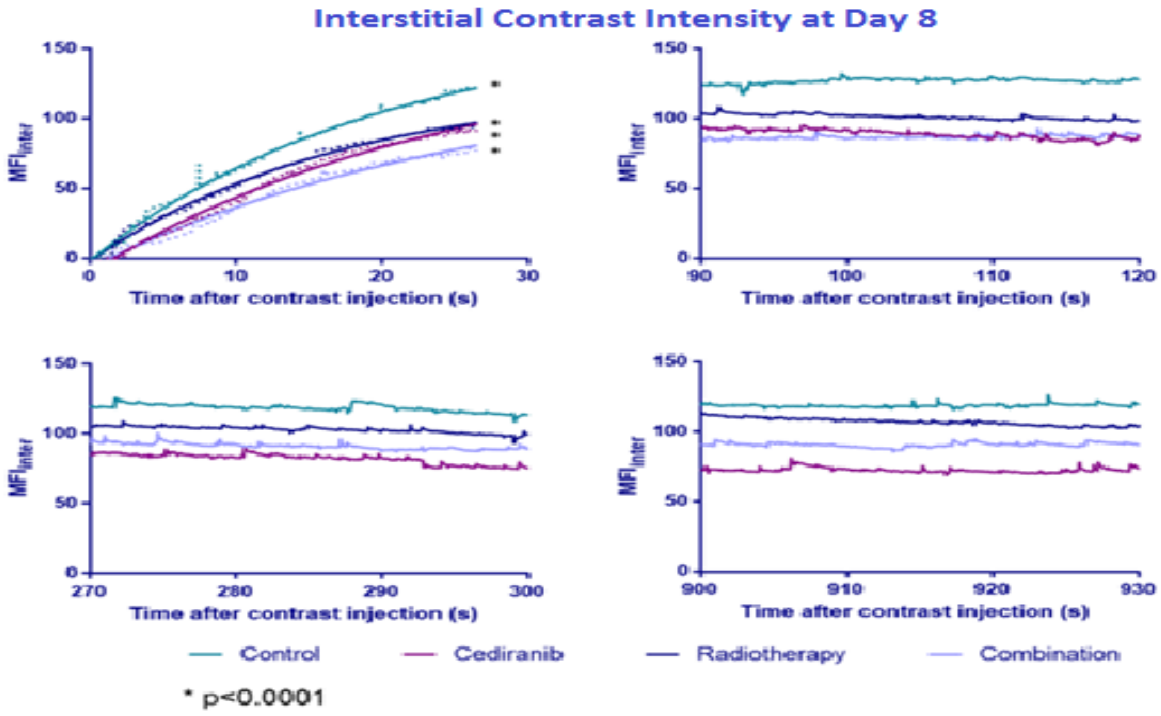

Graph 7

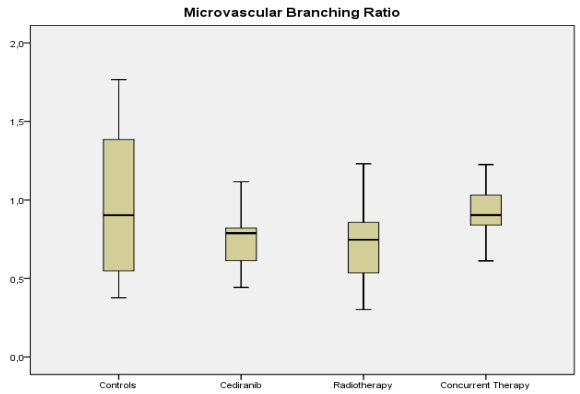

Graph 1

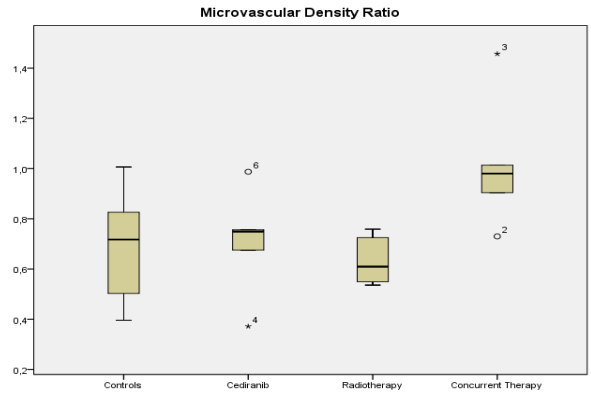

Graph 2

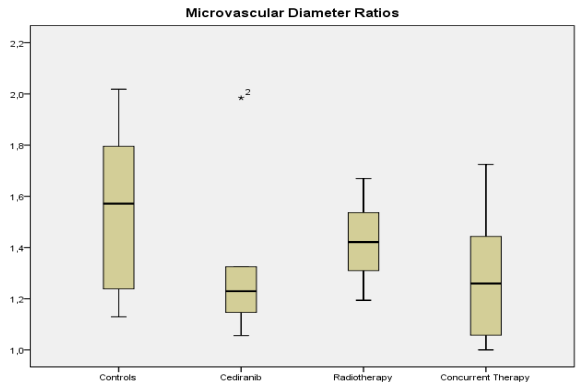

Graph 3

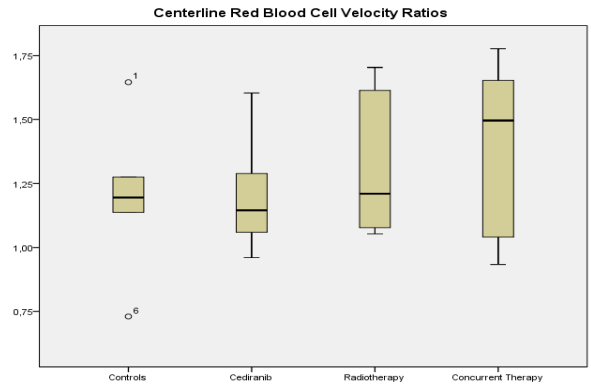

Graph 4

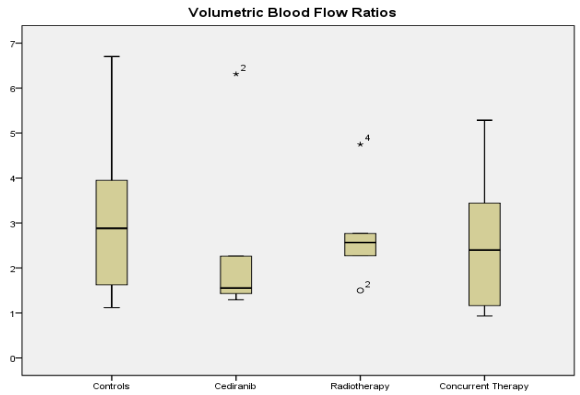

Graph 5

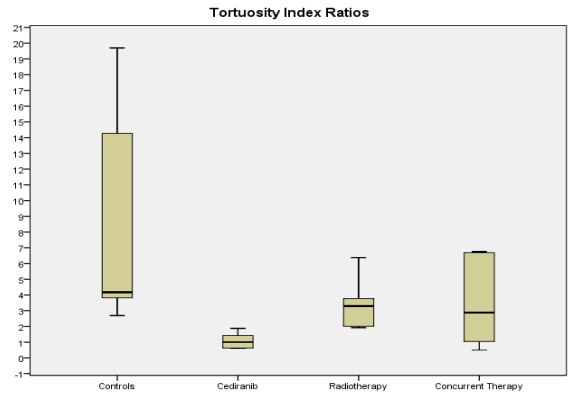

Graph 6

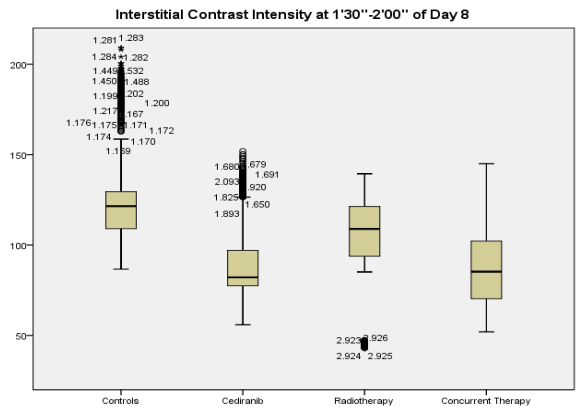

Graph 8

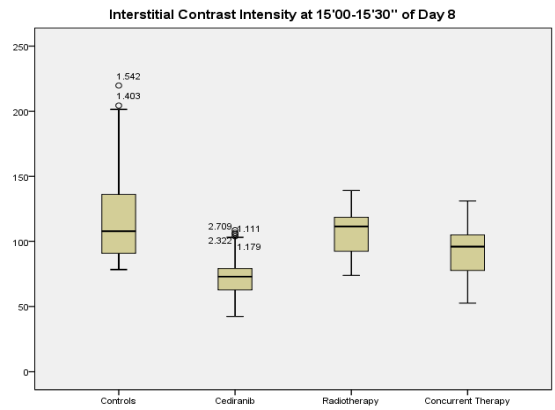

Graph 9

3.4 RESULTS SUMMARY

Although variable analyses were preceded by thoroughly elaborated outcome predictions, only two variables seemed to have shown a meaningful statistical significance. Different causes are deemed to explain the absence of statistical significance in the inferior. Yet table 22 summarizes the p-values of intergroup significant differences for each variable.

Results summary		
Variable	**Significant Intergroup difference**	**Interpretation controls to concurrent modality therapy**
N/A	P=0.543, not significant	Decrease, but unreliable
L/A	P=0.016, significant	Increase, but unreliable
D	P=0.427, not significant	Decrease
RBV	P=0.570, not significant	Increase
VQ	P=0.625, not significant	Decrease
Torq	P=0.012, significant*	Decrease (++)
Per (0'00"-0'-30")	P<0.001, significant**	Decrease (++)
Per (1'30"-2'00")	P<0.001, significant, between all groups (addendum 3)***	Decrease (++)
Per (15'00"-15'30")	P<0.001, significant, between all groups (addendum 3)****	Decrease (++)

**Controls (median: 4,17, Q1:3,540; Q3:15,619) to Cediranib monotherapy (median: 1,01, Q1:0,617; Q3:1,533) (P=0.002)*
***Regression plateau:*
=>Controls (166.9, CI95%: 156.6-177.2) to cediranib monotherapy (150.5*, CI95%:136.2-164.8) (P<0.001)*
=>Controls (166.9, CI95%: 156.6-177.2) to concurrent modality treatment (134.6*, CI95%:122.3-146.9) (P<0.001)*
=>Cediranib (150.5, CI95%:136.2-164.8) to Concurrent modality treatment (134.6*, CI95%:122.3-146.9) (P<0.001)*
**** Control group: median:122,035 (Q1:109,283;Q3:129,220); Cediranib group: median:82,140 (Q1:77,453;Q3:97,080); Radiotherapy group: median:108,620 (Q1:91,773;Q3:120,527) ; Concurrent modality group: median:84,890 (Q1:70,150; Q3:101,530)*
***** Control group: median:107,830 (Q1:90,85; Q3:136,058); Cediranib group: median:72,940; (Q1:62,732; Q3:79,205); Radiotherapy group: median:111,510; (Q1:92,490; Q3:118,558); Concurrent modality group: median:96,050; (Q1:77,662; Q3:104,988)*

Table 22

4. DISCUSSION

4.1 AIMS AND RESULTS, RELIABILITY AND LIMITATIONS

The aims were to investigate the effect of concurrent VEGF RTK inhibition and radiotherapy on microvascular structure and function. As a more thorough study of quantitative angiogenesis characteristics is not fully performed earlier (45, 51), specific vascular variables were defined and included. In vivo microscopic examinations of microvascular changes over a treatment regimen of 5 days were performed. Micro-environmental analyses and tumor growth experiments applying the same treatment regimens were executed as part of a larger project that was conducted by a PhD student. The project (including dorsal skinfold window experiments) was selected for a poster presentation at the Congres of the Society of Surgical Oncology 2016, Boston, US. Results presented in this paper are limited to the DSWC experiments. Nevertheless differences in microvascular patterns in the tumor singly seem to contribute to a higher treatment susceptibility. For instance, a conserved blood vessel perfusion and a transmembrane diffusion gradient are related to better oxygenation and drug delivery as seen earlier. On the other hand, uncontrolled and untreated tumor neovascularization is indicative of more malignant neoplasm. Hence micro-vessel characteristics show to be performant parameters for tumor growth control.

4.1.1 MICROVASCULAR BRANCHING

The microvascular branching, which was predicted to augment in the controls group, to remain the same in the cediranib monotherapy group and to decrease in the radiotherapy and the concurrent multimodal radiotherapy and cediranib group, did not show any significant difference. Possibly, the counting of each and every vessel branch over the whole microscopic field was compromised by tumor overgrowth and inflammatory edema in the controls group and irradiation necrosis in the radiotherapy group. In the cediranib group also a remarkable lowering of the vascular branching occurred. This is possibly explained by the following two paradigms: the ‘vascular shutdown’ effects of immature vessels by cediranib or coverage effects of inflammatory edema from the presence of excited small vessels in the cediranib group which impairs accurate vessel countings. A clinical trial by Batchelor et al. ,however, specifically investigated the effects of cediranib on tumor edema in gliomas. They showed a rapid decrease in tumor edema within 24h which lasted for at least 28 days of treatment.(85) Less edema and radionecrosis were expected and thus demonstrated in the concurrent modality treatment group. This is explained by sufficient oxygenation countering radionecrosis and destruction of

inflammatory excited small vessels countering edema. Hence more reliable data are accessible for the combined treatment group. In vivo microscopy on osteosarcoma xenografts revealed a significant increase in vascular branching for untreated tumors after two weeks of growth (49). Similar studies with histological counts for vascular branching demonstrated a significant decrease in vascular branches, starting at day 2 and continuing to day 21 for cediranib monotherapy (6mg/kg/d) in established lung cancer xenografts. (57). An unchanged ratio was demonstrated for fractionated radiotherapy in established prostate cancer xenografts. No relation to EC apoptosis was found (69). Significant differences in vascular branching were demonstrated in similar studies on lung cancer xenografts between concurrent modality treatment and controls. (51, 56)

4.1.2 Microvascular Density

Microvascular density analyses did show significant difference. These findings were however highly questionable, since some of the data seem to be extremely contradictory to a priori stated predictions. Again, a plausible explanation is a contrast masquerade by tumor overgrowth, edema and irradiation necrosis. Hence, since data for density analyses are very susceptible to each drawn line, less features were added to the controls, cediranib and radiotherapy groups than expected. Thus in controls and cediranib groups day 8 over day 0 change ratios of less than 1.0 were noted. This is indeed very questionable, since it is unlikely that any vessel destruction occurred. In vivo microscopy on osteosarcoma xenografts revealed a significant increase in vascular density for untreated tumors after two weeks of growth (49). Another study on established lung cancer xenografts demonstrated a significant decrease in vascular density, starting at day 2 and continuing to day 21 of cediranib monotherapy treatment(6mg/kg/d).(57) In our study an enormous decrease in vascular density in the radiotherapy group is seen as well. In the dosage used, this vast antivascular effect is counterintuitive. An unchanged ratio was demonstrated for fractionated radiotherapy in established prostate cancer xenografts whereas the controls nearly doubled. No relation to EC apoptosis was found (69) Studies using higher radiotherapeutic dosages evince large decreases in vascular density, starting from 12Gy dd.(71, 72, 86) On the other hand concurrent modality groups have well perfused vessels and less masquerades as explained in the above. This renders more vessel visibility and data reliability. Since small vessel destruction is performed by irradiation and cediranib is blocking radio-induced

neovascularization, the concurrent modality treatment group was expected to have the least day 8 over day 0 microvascular density change ratio.

4.1.3 Microvascular Diameter

Diameter analyses showed, however not significantly, to correspond better to a priori predictions. An overall increase was observed. A possible explanation is that a physiological dilatation is one of the first signs of endothelial cell instability. Hence it is observed in our study, however without significant proof, that microvessels in the VEGF RTK-inhibitor monotherapy group remain the least dilated. In a similar study on cediranib monotherapy also only a slight increase in vessel wall diameter was demonstrated in fibrosarcoma xenografts. (87) It is observed that increased diameters are more related to vessel wall instability than to small vessel destruction since the control group shows the highest microvascular diameter ratios. In an earlier study on fractionated radiotherapy (2Gy/d) though, no increased vessel diameter was seen in established prostate cancer xenografts. (69) A single dose of 30Gy in established cervical cancer xenografts showed an increased diameter. Also large vessels more likely remained intact while smaller vessel were destroyed. (69, 86) It could be expected that the radiotherapy group has the largest diameter since there is no VEGFR2 blockage and small vessels are destroyed. A comparison with the controls group showed however a larger mean diameter for the controls group. This indicates the both anti-angiogenic and angiogenic effects of fractionated radiotherapy. (72) An explanation for better reliability of these data is that for data acquisition of vessel diameters not each and every single vessel has to be measured and only a mean of randomly selected vessels is used.

4.1.4 Centerline Red Blood Cell Velocity

The data reliability of centerline red blood cell velocity is passed for the same criterion as in the diameter analyses, since only a few randomly selected vessels are included. By consequence the data respond better to a priori stated predictions. An overall increased velocity is seen in each treatment group. This is initially related to an overall microvascular diameter increase according to Poiseulle's law. Though a tendency to install a higher velocity in the VEGF-RTK inhibitor groups is observed. As suggested earlier, the centerline red blood cell velocity is more related to vessel wall stability and arterio-venous pressure gradients than vessel capacity.(46) In addition, the destruction of smaller vessels in the radiotherapy groups is related to a supplementary increase of the mean centerline red blood cell velocity since relatively more large vessels with higher capacities are included. In a similar study on established prostate cancer xenografts a

significantly increased perfusion after two weeks of fractionated radiotherapy treatment (2Gy/day) was demonstrated. (69) This was seen together with an increased pericyte coverage indicating some sort of anti-angiogenic effect. (69, 71, 72) In MRI studies on the effects of cediranib to vascular perfusion in Calu 3 and C6 glioma xenografts, a reduced perfusion is seen in the first 24h, probably associated to immediate diameter reduction, followed by an increased perfusion after 48h, explained by the shutdown of immature vessels.(88, 89)

4.1.5 VOLUMETRIC BLOOD FLOW

Regarding the volumetric blood flow, this variable can be presented as an indicator for the perfusion level in one single vessel. Hence, this has no relation to the global tumor perfusion. To quantitatively measure the global tumor perfusion, suggestions can be formulated to elaborate a formula involving the vascular density and the volumetric blood flow. As no actual predictions could be made about the volumetric blood flow, only post hoc hypothetic studies are demonstrative. These showed however no intergroup differences. After all, this variable was generated from two datasets that contradicted each other. Controls for example showed higher diameter ratios, rendering more capacity, and the combined modality group showed higher velocity ratios, rendering more perfusion velocity. Hence a comparably increased volumetric blood flow was observed in both the controls and in the concurrent modality treatment group. Vajkoczy et al formulate a plausible explanation:

> "…*In fact, tumors may have several mechanisms to maintain microvascular perfusion despite successful therapeutic reduction of vascular density, including individual vessel dilatation, increase of red blood cell velocity and recruitment of nonperfused microvessels. This view is supported by the results of intravital microscopic studies, demonstrating that I) dilatation of tumor vessels represents one of the major mechanisms to compensate for the natural, progressive intratumoral (central) perfusion failure in growing tumors and II) targeting of tumor angiogenesis through inhibition of the VEGF receptor Flk-1 is associated with a significant increase of red blood cell velocity and blood flow rate that, in part, compensates for the successful reduction of functional vascular density by 30% to 70%.",* (90)

To cope with this problem, the cediranib group was compared with concurrent modality treatment group. Since the mean microvascular diameter as well as the mean centerline red blood cell velocity are expected to be lower in the cediranib monotherapy group due to small vessel destruction and remained vessel wall stability, statistical comparison should show significant

difference to the concurrent treatment modality group. This however was not significant, but indicative.

4.1.6 Tortuosity Index

Further on, since the tortuosity index strongly represents the severity grade of angiogenic imbalance, as predicted, a restoration of(?) this balance leads to major visible differences in vessel tortuosity. Hence a strong and significant difference is noted between the controls group and VEGF-RTK monotherapy group. In vivo microscopy on osteosarcoma xenografts revealed a significant increase in vascular tortuosity for untreated tumors after two weeks of growth. (49) A similar study in fibrosarcoma xenografts has also demonstrated a smoother vessel appearance in cediranib monotherapy regimen.(87) Data acquisition for the tortuosity index is reliable because only a select amount of vessels were required for analysis. Remarkably, only a slight increase in tortuosity was seen in the radiotherapy monotherapy group, indicating that, beside its angiogenesis inducing effects, an additional antiangiogenic effect is noted. Earlier studies suggest that irradiation has an inhibitory effect on the proliferative compartment of the endothelial cells.(69, 72). In a study on established prostate cancer xenografts no change in tortuosity after two weeks of fractionated radiotherapy treatment (2Gy/day) was demonstrated. (69) This counters the a priori stated prediction of tortuous neovascularization following radiotherapy.

4.1.7 Permeability Index

The permeability index is a very sensitive variable rendering clear clues on subtle changes in VEGF-balance. Hence a high leakiness is observed in the controls group where severe disruption of the VEGF balance and thus high vessel wall instability is statistically demonstrated as predicted. The same quick increase and high slope for tumor microvasculature was described by Reitan et al. (49)

Also remarkably a quick significant increase in contrast extravasation is shown in the cediranib monotherapy group that stagnated again progressively, and finished significantly as the group with the least diffusion gradient. This is explained by the presence of a larger vascular bed filled with a large amount of small vessels which facilitates a quick increase in contrast intensity, but does not reach the diffusion peaks of the controls or radiotherapy group due to a more stable vessel wall. In the resolution phase the extravasation gradient of the cediranib-treated mice is significantly declined which renders following explanations: the occurrence of less contrast stasis

(by more efficient and less damaged vessels), an increased drainage (since drainage structures are not destroyed by radiotherapy), and a more stable vessel wall. These findings suggest a possible decreased IFP in the cediranib monotherapy group and a significantly greater adverse effect of irradiation destruction on drainage than VEGF-R3 lymphangiogenesis inhibition by cediranib. Reitan et al attributed a decrease in contrast intensity to vascular resorption or the outward convective gradient in tumors. (49)

The significantly less stable vessel wall in the concurrent modality group compared to the cediranib monotherapy group is explained by little radio-induced angiogenesis effects as mentioned in the introduction.
Additionally, as indicated by the study of Imaizuma et al (72), for vascular permeability also a remarkable counterintuitive statistical proof for the anti-angiogenic effects of fractionated radiotherapy is delivered. This ideology is plausible since peak extravasation (1’30’’-2’00’’) is a variable inherent to the angiogenesis balance and not related to the presence of small vessels. In a study on established prostate cancer xenografts, it was demonstrated that the microvascular permeability after two weeks of fractionated (2Gy/day) radiotherapy treatment did not change.(69) An MRI study on established colorectal cancer xenografts even demonstrated a significant decrease in vascular permeability after 5 days of fractionated radiotherapy (5Gy dd).(70) The permeability index is a reliable variable, since contrast intensity change is measured on select locations. In conclusion the permeability index is *chronologically* dependent on the amount of small vessels and the centerline red blood cell velocity followed by vessel wall stability and drainage capacity. This is confirmed by the research of Reitan et al. and Yuan et al., where permeability was associated to a higher fractal dimension, branching and density and lower red blood cell velocity. (49, 91)

4.2 OTHER CONSIDERATIONS ON RESULTS EXTRAPOLATION

4.2.1 NO CONSENSUS DOSAGES FOR RADIOTHERAPY AND CEDIRANIB

Some incentives were already given in the past on vascular modulatory effects of fractionated radiotherapy beneath 10 Gy. (73) No actual optimal irradiation dose was yet described. For this study a daily dose of 1.8 Gy seemed to exert inhibition of robust angiogenesis regarding the mean vasculature tortuosity analyses (as a trend) and inhibition of subtle angiogenesis regarding the mean vascular diameter (as a trend) and peak permeability index analyses ($P<0.001$) . We could not demonstrate a decrease in mean vascular density. So did a similar study using fractionated RT of 2Gy dd. (69)Higher dosages, even of 30Gy, also demonstrated beneficial effects of increased perfusion and reduced hypoxia, but consistently induced a significant decrease in mean vascular density. (70, 71, 86)

Cediranib dosage is determined following prescription of Astra Zeneca. In this study cediranib administration was maximally dosed to ascertain its antiangiogenic effect (61, 75) on robust angiogenesis effects (tortuosity index: $P<0.001$) and subtle changes (peak permeability index: $P<0.001$), however similar studies could prove significant tumor growth delaying effects at lower doses (56, 74, 76)

4.2.2 NO CONSENSUS PROTOCOL CAPIMAGE AND IMAGEJ

Data for microvascular branching, density, diameter and centerline red blood cell velocity were acquired through IVM analyses using CapImage. Although recent experience using this software is already provided (78, 79)), no actual protocol was formally at hand to efficiently perform operations on CapImage. By consequence, we explored and implemented our own findings on the applications and use of CapImage, with the help of colleagues and Dr. Zeintl, the creator of CapImage. Our proposals and provisory protocol on the use of CapImage are added in addendum 2. To measure the tortuosity index, ImageJ was used. For this software, descriptions of use were at hand. (81). For the permeability index, variable analyses were performed according to Patlak and Reitan (49, 82, 83), however no ratios to changes in intravascular contrast were calculated and analyzed. Though our graphs show to be consistent with the model of Patlak, since they show an irreversible state that eventually becomes linear, with a slope of constant contrast extravasation (K).

4.2.3 NO VARIABLE TRANSFORMATIONS USED

Although data were acquired to sometimes measure only small nuance differences, we still attempted to find significant statistical proof. This was in most of the cases not achieved and only some tendencies were examined. A logical operation would have been a variable transformation of some sort (square, square root, …). This, however, was not performed.

4.2.4 TESTING POWER

Another consideration on the compromised significant intergroup differences is the inadequate testing power for ANOVA tests. Hence only non-parametrical tests were performed. For $\alpha=0.05$ and $\beta=0.80$ and a small effect size, a relatively large sample is required. The primary outcome of the large project however, the tumor perfusion, was shown to have a sufficient sample size. Regarding this component of the large study though, each treatment group consisted of 6 individuals. For tortuosity index ratio and permeability index ratio no ANOVA test could be performed because of a non-parametrical distribution. For microvascular branching ratio and density ratio no conclusions could be made due to confounding by tumor overgrowth, edema and radionecrosis. For microvascular diameter ratio and centerline red blood cell velocity ratio the samples showed a normal distribution. However to perform a powerful parametrical analysis the sample sizes remained questionable. The microvascular diameter ratio of the control group had a mean of 1.55 and the concurrent modality group a mean of 1.29, with a pooled SD of 0.312. Thus to adhere statistical power a sample size of minimum 60 individuals was required. Applying the same procedure for the centerline RBC velocity ratio, with $\mu1= 1.20$ and $\mu2=1.40$ and a pooled SD of 0.316, 39 individuals were actually needed.

4.2.5 TUMOR SIZE

A limitation to the application of DSWC models is the restriction of tumor growth. It is seen that a tumor grown in DSWC restricts to maximally 100mm². For studies examining growth delay, the quadrupling time (RTV4) is a valuable variable. To reach RTV4 a tumor has to grow to over 700 to 1100mm². In addition in larger tumors a different stroma constitution may alter IFP and necrosis variances, leading to interpretation dissimilarities. Hence the applicability of DSWC is confined to studies at the early tumor phases, (51) rendering opportunities for nascent angiogenesis studies (anti-VEGF) but not for studies on angiogenesis resolution such as Ang-2.(92) After all, the initially observed antiangiogenic effects of antiVEGF seem to vanish at day

6, terminating the ‘therapeutic window’ and turning the ‘angiogenic switch’ from normalization to anti-vascular. (51)

4.3 INTERPRETATION AND IMPLICATIONS FOR TREATMENT

As previously described, aberrant tumor neovascularization leads to an increased IFP, heterogeneous hypoxia and acidosis. These conditions create a hostile environment fueling tumor metastatic capacity and invasiveness and treatment resistance. An attempt to explain a potential resolution or worsening of the malign tumor micro-environment in the respective treatment groups is done through analysis of microvascular structure and function. Table 23 summarizes our findings: ‘1’ is the control group, ‘2’ the cediranib monotherapy group, ‘3’ the radiotherapy monotherapy group, ‘4’ the concurrent modality treatment group.

4.3.1 UNIFORM OXYGEN AND METABOLITES DELIVERY

To obtain uniform oxygen and metabolites delivery, a conserved fractal-like perfusion is needed. Two parameters measuring vessel perfusion are centerline red blood cell velocity and volumetric perfusion . (79) Our results suggest that the mean centerline red blood cell velocity is increased in the concurrent treatment modality group compared to the controls group. Also, studies on cediranib monotherapy demonstrated an increased vessel perfusion. (88, 89) Other studies demonstrated an increased perfusion and alleviated hypoxia following fractionated radiotherapy treatment.(69-71) When generalizing this observation, an increased uniform oxygen and metabolites delivery during the ‘normalization window’ is guaranteed. Additionally the use of a percolation model could deliver incentives on a ‘normalized’ fractal like homogeneous blood supply.(83) This is discussed in the future perspectives section.

4.3.2 IFP

A physiologic IFP depends on vessel wall stability, drainage potential and reduced external mechanic pressure. Variables contributing to vessel wall stability are the vascular diameter (79) and permeability at peak extravasation (49). The vascular diameter and vascular permeability (significantly) show to be reduced in the RTK inhibitor groups and even, however counter-intuitively, in the radiotherapy groups, indicating the presence of angiogenesis inhibition. Increased drainage potential is related to contrast intensity characteristics.(49) A progressive decline in contrast intensity was statistically demonstrated in the cediranib monotherapy group,

other groups showed no change. This is possibly explained by a primordially reduced IFP during the treatment course enhancing vascular resorption, lymphatic drainage and/or the outward convective gradient in the tumor interstitium. Variables related to external mechanic pressure are centerline red blood cell velocity and volumetric blood flow. These are discussed in the former section. Hence a transient decrease in IFP is suggested for the cediranib monotherapy group and the concurrent modality treatment group, generating a 'window of opportunity' for pharmaceutical metabolites delivery to the tumor micro-environment.

Micro-environment Changes					
Uniform oxygen and metabolites delivery		1	2	3	4
Vascular aspects	Variables selection				
-*Vessel Perfusion*	Centerline RBC velocity Ratio	+	+	++	+++
	Volumetric Blood Flow Ratio	+++	+	++	++
-*Fractalization*	Percolation Models	*Future Perspectives*			
IFP		1	2	3	4
Vascular aspects	Variables selection				
-*Vessel Wall Instability*	Diameter Ratio	+++	+	++	+
	Permeability Index after 1'30'' (Peak extravasation)	+++*	+*	++*	+*
-*Drainage Obstruction*	Permeability Index after 15'00'' (Resolution extravasation)	Constant*	Reduce*	Constant*	Constant*
-*Relieved Mechanic Pressure*	Centerline RBC velocity Ratio	+	+	++	+++
	Volumetric Blood Flow Ratio	+++	+	++	++

Table 23 : *significant intergroup difference (P<0.001)

4.3.3 Clinical Use

The translation of these findings into practical clinical use warrants further investigation. At least these results give interesting additional quantitative support to recent clinical trials that have been testing vascular normalization and resistance to antiVEGF therapy in distinct clinical tumor types. Pioneering clinical research on tumor microvascular normalization was performed in 2004 by Willet et al. They found an increased vessel maturation and decreased IFP in rectum carcinomas after a single infusion with bevacizumab.(93) Later on, recurrent and newly

diagnosed glioblastomas multiforme (GBM) were investigated for microvascular normalization. The add-on treatment of cediranib to chemoradiation in GBM lead to an increased tumor perfusion and decreased edema on MRI and a subsequent oxygenation in a subset of the treated patients. In these patients the vascular normalization effects alone already lead to an increased survival. (94-96) It is seen that it has no use to continue the expensive treatment with cediranib when no early oxygenation and perfusion can be demonstrated. Additionally the presence of VEGFR1 and IL8 in the blood plasma of the patient are adversely predictive for treatment success. (94, 97) Also, as mentioned in the introduction, several trials with cediranib combined to FOLFOX/CAPOX chemotherapy were conducted in metastatic colorectal cancer patients groups. These however showed little to no benefits on progression free survival.

4.4 PROS AND CONS: RELATION TO SIMILAR STUDIES

To estimate the practical value of this study a comparison is made to similar publications. An extensive search on pubmed and google scholar for comparable studies on combined use of cediranib and radiotherapy and DSWC models for in vivo imaging resulted in two search results. A study from 2007 by Wiliams KJ et al. and a thesis from Brian Telfer. Supposedly the two authors discuss the same experiment since Telfer is co-author in the article of Williams KJ. A more extended description of the experiment though is delivered by Telfer. Only qualitative analyses by brightfield IVM were performed. Outcomes were described as “change from a multi-branched appearance to fewer branching vessels 48h later. This change continued with some vessels either closing or disappearing over successive imaging days resulting in smoother vessel appearance compared to that seen on treatment day 0.” (51) We can reformulate this as small vessel destruction and decreased density, tortuosity and diameter, consolidated by cediranib administration. A comparison with the study of Williams et al. is given in table 23. In the publication by Williams et al. additional histologic analyses were performed to quantitatively measure changes in vascular branching for the same treatment regimens. They found a reduced branching in the sequentially treated group (6 ± 0.4 vessels per mm^2) compared to the monotherapy groups and the concomitant modality treatment group (8 ± 1 per mm^2); ($P = 0.02$). (75) No conclusion can be made for which treatment regimen is more adequate. Globally the same tendency is observed.

4.4.1 SARRP

Our study also prevails in its radiotherapeutic precision using the specially designed SMALL ANIMAL RADIATION RESEARCH PLATFORM (SARRP). This device allows confident 0.5 mm beams for precise research inquiries on selected anatomical locations. Hence more isolated tissue observations are possible. (98)

Study comparison RT, cediranib and DSWC		
	Williams et al, 2007	Our study
Material and methods	Lung: Calu-6 tumor cell line Radiotherapy (6 Gy in 3 fractions daily, no anesthesia), followed by cediranib (3mg/kg daily), 3 consecutive days	Colon: HT29 tumor cell line Cediranib 6mg/kg, oral gavage 1x dd (2h pre-RT) followed by radiotherapy under anesthesia, 1,8 Gy 1x dd, 5 consecutive days
Design	3 treatment groups: vehicle (n=2), cediranib (n=2), concurrent modality (n=2)	4 treatment groups: vehicle (n=6), cediranib (n=6), radiotherapy (n=6), concurrent modality (n=6)
Data acquisition	Qualitative analyses, in vivo brightfield microscopy in DSWC models, eyeball method	Quantitative analyses, in vivo fluorescence laser microscopy in DSWC models, imaging and analyzing software

Table 23

4.4.2 DATA ACQUISITION

Another asset of this study is the manually performed data acquisition from IVM videos in CapImage and ImageJ. Thus every visible vessel is included. However Maeda described digital methods in ImageJ using smoothing and skeletonisation plugins for branching, density and tortuosity, these pixel based adaptations are not yet as precise. (99)

4.5 FUTURE PERSPECTIVES FOR DORSAL SKINFOLD WINDOW CHAMBER RESEARCH

Referring to our limitations and suggestions from literature some implications for future research in DSWC and vascular normalization are presented.

4.5.1 TUMOR CELL SUSPENSION INJECTION

From experience in the contemporary study, we concluded to adopt the injection technique instead of the implantation technique. The technique of implantation is more complex (donor animals are needed) and moreover, the implanted graft tended to generate tissue inflammation, compromising qualitative and reliable analysis.

4.5.2 OPTICAL FREQUENCY DOMAIN REFLECTOMETRY (=OFDR)

Next to the experiments of Tozer et al. using multiphoton microscopy for quantitative in vivo analyses, rendering options of 3D reconstruction for fractal analyses of the vasculature and/or coping with confounders, (83)also the development of the OFDR, which renders an even greater penetration depth and consolidated resolution, has promising implications for DSWC research. (46) 3D fractal analyses generate possibilities to compare *in vivo* observations to mathematical "percolation models" or "diffusion-limited" fractal models, where stochastical obstructions impede further fractalization. In this way a new variable to quantitatively analyze vascular normalization against heterogeneous oxygen and metabolite supply by tumor angiogenesis is created. (83)

4.5.3 ANALYZING PROTOCOL

To standardize data acquisition from the DSWC, it is mandatory to use a common analyzing protocol. The protocol used in this study, is a good kick start for future elaboration. The protocol is added in addendum 2.

4.5.4 COMPATIBILITY PRECLINICAL AND CLINICAL RESEARCH

Different barriers generally impeding the complementary between preclinical and clinical studies are described by Jain 2014. (97)

First, most tumor grafts in murine models have rapid growth potential and are highly susceptible to anti-VEGF treatment. Furthermore genetically engineered mice (GEMM) show no potency to evolve tumor metastasis, therefore new models are being developed with a 'humanized' immune system. In this study human xenograft models were used which indeed represent more realistic

insights in tumor angiogenesis.
Second, the administration of anti-VEGF treatment in humans confers survival benefits for metastasized cancer and is applied as adjuvant therapy. In preclinical models however, mostly primary tumors are treated in a neoadjuvant treatment regimen. Programs to develop advanced metastatic cancer types for murine models are being investigated. (100)
Third, it often occurs that the anti-angiogenic dosage in preclinical studies is too high. For higher doses of VEGF antibody (bevacizumab), no adverse effects were noted. For RTK-inhibitors, and specifically sunitinib, at high doses, increased permeability and metastatic capacity were seen since RTK's involved in EC-junction mechanisms also became affected. (101)
Fourth, instead of intervention strategies, studies in genetically engineered mouse models (GEMM) often investigate prevention strategies, since GEMM are expected to spontaneously evolve cancer. Hence findings may not be translatable and can even derail treatment regimens. In this study CRC is induced and grown for 7 days to install a typical tumor microvasculature. Our treatment regimen started already at day 2 so a prevention strategy for tumor angiogenesis was investigated.

4.5.5 Vascular Normalization and Immunotherapy

It is also presumed that vascular normalization enhances immunotherapies of any kind (46)Resolving the hostile tumor microenvironment elicits more efficient lymphocyte infiltration, upregulation of immune check-point protein expression via hypoxia, recruitment of Tregs, activation of resident and transiting immune effector cells in the tumor environment, otherwise suppressed by VEGF. No actual relation between vascular normalization and immunotherapy enhancement has yet been demonstrated. (102)No immunologic effects were of notifiable relevance in this study since immune incompetent athymic mice models were used to grow CRC.

4.5.6 Toxicity of anti-angiogenic drugs

However it needs to come to our attention at any time that anti-VEGF treatment is not without toxic side effects. Therefore the benefits on patient survival have to be measured against potential toxicity. Faruque et al. conducted a systematic review on adverse effects of VEGF inhibition, they resumed the number needed to harm ranges from 7 to 125. The most common side effects were cardiovascular: MI, hypertension, arterial thromboembolism and non-cardiovascular proteinuria, delayed wound healing, gastrointestinal perforation. (103) Furthermore the HORIZON III (HORIZON) trial and Cunningham et al demonstrated that the administration of

cediranib rendered no overall survival benefits compared to bevacizumab because of possible side effects.

4.6 CONCLUSION

Quantitative analyses of tumor microvascular structure and function were conducted through intravital microscopy in dorsal skinfold window chambers. Microvascular branching, density, diameter, centerline red blood cell velocity, volumetric blood flow, tortuosity and permeability were examined. Through examining significant differences between treatment groups, we attempted to assort objectified instructions for future studies on normalization. Although some remarkable variable tendencies were noted, only statistical significance could be delivered to measurements on vascular tortuosity and permeability. Considerations on results extrapolation are extensively discussed.

5. REFERENCES

1. Ferlay J, Steliarova-Foucher E, Lortet-Tieulent J, Rosso S, Coebergh JW, Comber H, et al. Cancer incidence and mortality patterns in Europe: estimates for 40 countries in 2012. Eur J Cancer. 2013;49(6):1374-403.
2. Siegel R, DeSantis C, Jemal A. Colorectal cancer statistics, 2014. CA: A Cancer Journal for Clinicians. 2014;64(2):104-17.
3. Luengo-Fernandez R, Leal J, Gray A, Sullivan R. Economic burden of cancer across the European Union: a population-based cost analysis. Lancet Oncol. 2013;14(12):1165-74.
4. Bonelli L. Epidemiology and screening: what's new? Colorectal Disease. 2015;17:10-4.
5. Society. AC. Colorectal Cancer Facts & Figures 2014-2016.

. Atlanta: 2014.
6. Church J. Hereditary colorectal cancer. The ASCRS Manual of Colon and Rectal Surgery: Springer; 2014. p. 697-733.
7. Grady WM, Carethers JM. Genomic and Epigenetic Instability in Colorectal Cancer Pathogenesis. Gastroenterology. 2008;135(4):1079-99.
8. Society AC. How is colorectal cancer diagnosed? 2015 [cited 2015 2 Decembre]. Available from: http://www.cancer.org/cancer/colonandrectumcancer/detailedguide/colorectal-cancer-staged.
9. Schnekenburger M, Diederich M. Epigenetics Offer New Horizons for Colorectal Cancer Prevention. Curr Colorectal Cancer Rep. 2012;8(1):66-81.
10. Reuter S, Gupta SC, Chaturvedi MM, Aggarwal BB. Oxidative stress, inflammation, and cancer: How are they linked? Free Radical Biology and Medicine. 2010;49(11):1603-16.
11. Ries LAG, Melbert D, Krapcho M, Stinchcomb D, Howlader N, Horner M, et al. SEER cancer statistics review, 1975–2005. Bethesda, MD: National Cancer Institute. 2008:1975-2005.
12. Ekbom A, Helmick C, Zack M, Adami HO. Ulcerative colitis and colorectal cancer. A population-based study. N Engl J Med. 1990;323(18):1228-33.
13. Johnson CM, Wei C, Ensor JE, Smolenski DJ, Amos CI, Levin B, et al. Meta-analyses of colorectal cancer risk factors. Cancer Causes & Control. 2013;24(6):1207-22.
14. Research IAfC. Colorectal Cancer: Estimated Incidence, Mortality and Prevalence Worldwide in 2012 2012. Available from: http://globocan.iarc.fr/Pages/fact_sheets_cancer.aspx?cancer=colorectal.
15. Flood DM, Weiss NS, Cook LS, Emerson JC, Schwartz SM, Potter JD. Colorectal cancer incidence in Asian migrants to the United States and their descendants. Cancer Causes & Control. 2000;11(5):403-11.
16. Conwell T, Boscoe FP. Urban/rural disparities in cancer incidence in New York State, 2008-2012. PeerJ PrePrints, 2015 2167-9843.
17. Zauber AG, Winawer SJ, O'Brien MJ, Lansdorp-Vogelaar I, van Ballegooijen M, Hankey BF, et al. Colonoscopic Polypectomy and Long-Term Prevention of Colorectal-Cancer Deaths. New England Journal of Medicine. 2012;366(8):687-96.
18. Heresbach D, Manfredi S, D'Halluin P N, Bretagne JF, Branger B. Review in depth and meta-analysis of controlled trials on colorectal cancer screening by faecal occult blood test. Eur J Gastroenterol Hepatol. 2006;18(4):427-33.
19. VZW Cvk. Bevolkingsonderzoek dikke darmkanker 2013. Available from: https://www.bevolkingsonderzoek.be/dikkedarmkanker/professionelen-motivatie-keuze-van-de-iFOB-test.
20. Lansdorp-Vogelaar I, Knudsen AB, Brenner H. Cost-effectiveness of colorectal cancer screening. Epidemiologic reviews. 2011;33(1):88-100.
21. Blanco GDV, Paoluzi OA, Sileri P, Rossi P, Sica G, Pallone F. Familial colorectal cancer screening: When and what to do? World journal of gastroenterology: WJG. 2015;21(26):7944.
22. Rex DK, Johnson DA, Anderson JC, Schoenfeld PS, Burke CA, Inadomi JM. American College of Gastroenterology Guidelines for Colorectal Cancer Screening 2008. Am J Gastroenterol. 2009;104(3):739-50.
23. Edge SB, Compton CC. The American Joint Committee on Cancer: the 7th edition of the AJCC cancer staging manual and the future of TNM. Annals of surgical oncology. 2010;17(6):1471-4.
24. O'Connell JB, Maggard MA, Ko CY. Colon cancer survival rates with the new American Joint Committee on Cancer sixth edition staging. Journal of the National Cancer Institute. 2004;96(19):1420-5.
25. Lacy AM, García-Valdecasas JC, Delgado S, Castells A, Taurá P, Piqué JM, et al. Laparoscopy-assisted colectomy versus open colectomy for treatment of non-metastatic colon cancer: a randomised trial. The Lancet. 2002;359(9325):2224-9.

26. Zheng Z, Jemal A, Lin CC, Hu C-Y, Chang GJ. Comparative Effectiveness of Laparoscopy vs Open Colectomy Among Nonmetastatic Colon Cancer Patients: An Analysis Using the National Cancer Data Base. Journal of the National Cancer Institute. 2015;107(3).
27. Sargent D, Sobrero A, Grothey A, O'Connell MJ, Buyse M, Andre T, et al. Evidence for cure by adjuvant therapy in colon cancer: observations based on individual patient data from 20,898 patients on 18 randomized trials. Journal of Clinical Oncology. 2009;27(6):872-7.
28. Rullier E, Denost Q, Vendrely V, Rullier A, Laurent C. Low Rectal Cancer: Classification and Standardization of Surgery. Diseases of the Colon & Rectum. 2013;56(5):560-7.
29. Heald RJ, Moran BJ, Ryall RH, Sexton R, MacFarlane JK. Rectal cancer: The basingstoke experience of total mesorectal excision, 1978-1997. Archives of Surgery. 1998;133(8):894-8.
30. Martin ST, Heneghan HM, Winter DC. Systematic review of outcomes after intersphincteric resection for low rectal cancer. British Journal of Surgery. 2012;99(5):603-12.
31. Mulsow J, Winter DC. Sphincter preservation for distal rectal cancer--a goal worth achieving at all costs? World J Gastroenterol. 2011;17(7):855-61.
32. DeSantis CE, Lin CC, Mariotto AB, Siegel RL, Stein KD, Kramer JL, et al. Cancer treatment and survivorship statistics, 2014. CA: A Cancer Journal for Clinicians. 2014;64(4):252-71.
33. Marques I, Araujo A, de Mello RA. Anti-angiogenic therapies for metastatic colorectal cancer: current and future perspectives. World J Gastroenterol. 2013;19(44):7955-71.
34. Feng Q-Y, Wei Y, Chen J-W, Chang W-J, Ye L-C, Zhu D-X, et al. Anti-EGFR and anti-VEGF agents: Important targeted therapies of colorectal liver metastases. World journal of gastroenterology: WJG. 2014;20(15):4263.
35. Neoadjuvant Treatment in Rectal Cancer: Actual Status. Chemotherapy Research and Practice. 2011;2011.
36. Leonard GD, Brenner B, Kemeny NE. Neoadjuvant chemotherapy before liver resection for patients with unresectable liver metastases from colorectal carcinoma. Journal of Clinical Oncology. 2005;23(9):2038-48.
37. Patan S. Vasculogenesis and angiogenesis. Cancer Treat Res. 2004;117:3-32.
38. Paku S. Current concepts of tumor-induced angiogenesis. Pathol Oncol Res. 1998;4(1):62-75.
39. Ausprunk DH, Folkman J. Migration and proliferation of endothelial cells in preformed and newly formed blood vessels during tumor angiogenesis. Microvascular research. 1977;14(1):53-65.
40. Cook KM, Figg WD. Angiogenesis inhibitors: current strategies and future prospects. CA: a cancer journal for clinicians. 2010;60(4):222-43.
41. Chung AS, Lee J, Ferrara N. Targeting the tumour vasculature: insights from physiological angiogenesis. Nat Rev Cancer. 2010;10(7):505-14.
42. Jain RK. Normalization of tumor vasculature: an emerging concept in antiangiogenic therapy. Science. 2005;307(5706):58-62.
43. Jain RK. Transport of molecules in the tumor interstitium: a review. Cancer Res. 1987;47(12):3039-51.
44. Jain RK. Normalizing tumor vasculature with anti-angiogenic therapy: a new paradigm for combination therapy. Nature medicine. 2001;7(9):987-9.
45. Jain RK. Normalizing tumor microenvironment to treat cancer: bench to bedside to biomarkers. Journal of Clinical Oncology. 2013;31(17):2205-18.
46. Fukumura D, Duda DG, Munn LL, Jain RK. Tumor Microvasculature and Microenvironment: Novel Insights Through Intravital Imaging in Pre-Clinical Models. Microcirculation (New York, NY : 1994). 2010;17(3):206-25.
47. Algire GH. An Adaptation of the Transparent-Chamber Technique to the Mouse. Journal of the National Cancer Institute. 1943;4(1):1-11.
48. Buades A, Coll B, Morel JM. A Review of Image Denoising Algorithms, with a New One. Multiscale Modeling & Simulation. 2005;4(2):490-530.
49. Reitan NK, Thuen M, Goa PE, de Lange Davies C. Characterization of tumor microvascular structure and permeability: comparison between magnetic resonance imaging and intravital confocal imaging. Journal of Biomedical Optics. 2010;15(3):036004.
50. Teicher BA. Role of angiogenesis in the response to anticancer therapies. Drug Resist Updat. 1998;1(1):59-61.
51. Telfer BA. Application of the dorsal window chamber to tumour vasculature manipulation studies.: The University of Manchester; 2012.
52. Dewhirst MW, Cao Y, Li CY, Moeller B. Exploring the role of HIF-1 in early angiogenesis and response to radiotherapy. Radiotherapy and Oncology. 2007;83(3):249-55.

53. Gorski DH, Beckett MA, Jaskowiak NT, Calvin DP, Mauceri HJ, Salloum RM, et al. Blockade of the vascular endothelial growth factor stress response increases the antitumor effects of ionizing radiation. Cancer research. 1999;59(14):3374-8.
54. Geng L, Donnelly E, McMahon G, Lin PC, Sierra-Rivera E, Oshinka H, et al. Inhibition of vascular endothelial growth factor receptor signaling leads to reversal of tumor resistance to radiotherapy. Cancer Res. 2001;61(6):2413-9.
55. Winkler F, Kozin SV, Tong RT, Chae SS, Booth MF, Garkavtsev I, et al. Kinetics of vascular normalization by VEGFR2 blockade governs brain tumor response to radiation: role of oxygenation, angiopoietin-1, and matrix metalloproteinases. Cancer Cell. 2004;6(6):553-63.
56. Cao C, Albert JM, Geng L, Ivy PS, Sandler A, Johnson DH, et al. Vascular endothelial growth factor tyrosine kinase inhibitor AZD2171 and fractionated radiotherapy in mouse models of lung cancer. Cancer Res. 2006;66(23):11409-15.
57. Wedge SR, Kendrew J, Hennequin LF, Valentine PJ, Barry ST, Brave SR, et al. AZD2171: A Highly Potent, Orally Bioavailable, Vascular Endothelial Growth Factor Receptor-2 Tyrosine Kinase Inhibitor for the Treatment of Cancer. Cancer Research. 2005;65(10):4389-400.
58. Actueel SG. Cediranib en Olaprib 2016. Available from: http://kanker-actueel.nl/olaparib-plus-cedinarib-lijkt-doorbraak-bij-controle-van-vergevorderde-eierstokkanker-en-verdubbelt-progressievrije-overleving-van-92-maanden-naar-177-maanden.html.
59. Lorusso P, Shields AF, Gadgeel S, Vaishampayan U, Guthrie T, Puchalski T, et al. Cediranib in combination with various anticancer regimens: results of a phase I multi-cohort study. Invest New Drugs. 2011;29(6):1395-405.
60. Satoh T, Yamaguchi K, Boku N, Okamoto W, Shimamura T, Yamazaki K, et al. Phase I results from a two-part Phase I/II study of cediranib in combination with mFOLFOX6 in Japanese patients with metastatic colorectal cancer. Invest New Drugs. 2012;30(4):1511-8.
61. Sciences NCfAT. AstraZenica AZD2171 (Cediranib) [cited 2015 14-12]. Available from: https://ncats.nih.gov/files/AZD2171.pdf.
62. Agency EM. On 29 July 2014, orphan designation (EU/3/14/1303) was granted by the European Commission to AstraZeneca AB, Sweden, for cediranib for the treatment of ovarian cancer.: European Union; 2014 [cited 2016]. Available from: http://www.ema.europa.eu/ema/index.jsp?curl=pages/medicines/human/orphans/2014/09/human_orphan_001381.jsp&mid=WC0b01ac058001d12b.
63. Hoff PM, Hochhaus A, Pestalozzi BC, Tebbutt NC, Li J, Kim TW, et al. Cediranib plus FOLFOX/CAPOX versus placebo plus FOLFOX/CAPOX in patients with previously untreated metastatic colorectal cancer: a randomized, double-blind, phase III study (HORIZON II). J Clin Oncol. 2012;30(29):3596-603.
64. Kato T, Muro K, Yamaguchi K, Bando H, Hazama S, Amagai K, et al. Cediranib in combination with mFOLFOX6 in Japanese patients with metastatic colorectal cancer: results from the randomised phase II part of a phase I/II study. Ann Oncol. 2012;23(4):933-41.
65. Schmoll HJ, Cunningham D, Sobrero A, Karapetis CS, Rougier P, Koski SL, et al. Cediranib with mFOLFOX6 versus bevacizumab with mFOLFOX6 as first-line treatment for patients with advanced colorectal cancer: a double-blind, randomized phase III study (HORIZON III). J Clin Oncol. 2012;30(29):3588-95.
66. Cunningham D, Wong RP, D'Haens G, Douillard JY, Robertson J, Stone AM, et al. Cediranib with mFOLFOX6 vs bevacizumab with mFOLFOX6 in previously treated metastatic colorectal cancer. Br J Cancer. 2013;108(3):493-502.
67. Garcia-Barros M, Paris F, Cordon-Cardo C, Lyden D, Rafii S, Haimovitz-Friedman A, et al. Tumor response to radiotherapy regulated by endothelial cell apoptosis. Science. 2003;300(5622):1155-9.
68. Hori K, Saito S, Tamai M. Effect of irradiation on neovascularization in rat skinfold chambers: implications for clinical trials of low-dose radiotherapy for wet-type age-related macular degeneration. International Journal of Radiation Oncology* Biology* Physics. 2004;60(5):1564-71.
69. Potiron VA, Abderrahmani R, Clement-Colmou K, Marionneau-Lambot S, Oullier T, Paris F, et al. Improved functionality of the vasculature during conventionally fractionated radiation therapy of prostate cancer. PloS one. 2013;8(12):e84076.
70. Ceelen W, Smeets P, Backes W, Van Damme N, Boterberg T, Demetter P, et al. Noninvasive monitoring of radiotherapy-induced microvascular changes using dynamic contrast enhanced magnetic resonance imaging (DCE-MRI) in a colorectal tumor model. International journal of radiation oncology, biology, physics. 2006;64(4):1188-96.
71. Lan J, Wan XL, Deng L, Xue JX, Wang LS, Meng MB, et al. Ablative hypofractionated radiotherapy normalizes tumor vasculature in lewis lung carcinoma mice model. Radiation research. 2013;179(4):458-64.

72. Imaizumi N, Monnier Y, Hegi M, Mirimanoff RO, Ruegg C. Radiotherapy suppresses angiogenesis in mice through TGF-betaRI/ALK5-dependent inhibition of endothelial cell sprouting. PloS one. 2010;5(6):e11084.
73. Park HJ, Griffin RJ, Hui S, Levitt SH, Song CW. Radiation-Induced Vascular Damage in Tumors: Implications of Vascular Damage in Ablative Hypofractionated Radiotherapy (SBRT and SRS). Radiation research. 2012;177(3):311-27.
74. Williams KJ, Telfer BA, Shannon AM, Babur M, Stratford IJ, Wedge SR. Inhibition of vascular endothelial growth factor signalling using cediranib (RECENTIN; AZD2171) enhances radiation response and causes substantial physiological changes in lung tumour xenografts. Br J Radiol. 2008;81 Spec No 1:S21-7.
75. Williams KJ, Telfer BA, Shannon AM, Babur M, Stratford IJ, Wedge SR. Combining radiotherapy with AZD2171, a potent inhibitor of vascular endothelial growth factor signaling: pathophysiologic effects and therapeutic benefit. Molecular cancer therapeutics. 2007;6(2):599-606.
76. Bozec A, Formento P, Lassalle S, Lippens C, Hofman P, Milano G. Dual inhibition of EGFR and VEGFR pathways in combination with irradiation: antitumour supra-additive effects on human head and neck cancer xenografts. Br J Cancer. 2007;97(1):65-72.
77. Laschke MW, Vollmar B, Menger MD. The dorsal skinfold chamber: window into the dynamic interaction of biomaterials with their surrounding host tissue. Eur Cell Mater. 2011;22:147-64; discussion 64-7.
78. Debergh I, Pattyn P, Ceelen W. Microvascular effects of the low molecular weight heparins in a colorectal xenograft model: an intravital microscopy study. J Surg Res. 2015;194(2):488-95.
79. Laschke MW, Elitzsch A, Vollmar B, Menger MD. In vivo analysis of angiogenesis in endometriosis-like lesions by intravital fluorescence microscopy. Fertility and Sterility. 2005;84, Supplement 2:1199-209.
80. Baker M, Wayland H. On-line volume flow rate and velocity profile measurement for blood in microvessels. Microvascular research. 1974;7(1):131-43.
81. Norrby K. Microvascular density in terms of number and length of microvessel segments per unit tissue volume in mammalian angiogenesis. Microvascular research. 1998;55(1):43-53.
82. Patlak CS, Blasberg RG, Fenstermacher JD. Graphical evaluation of blood-to-brain transfer constants from multiple-time uptake data. J Cereb Blood Flow Metab. 1983;3(1):1-7.
83. Tozer GM, Ameer-Beg SM, Baker J, Barber PR, Hill SA, Hodgkiss RJ, et al. Intravital imaging of tumour vascular networks using multi-photon fluorescence microscopy. Adv Drug Deliv Rev. 2005;57(1):135-52.
84. Ghasemi A, Zahediasl S. Normality Tests for Statistical Analysis: A Guide for Non-Statisticians. International Journal of Endocrinology and Metabolism. 2012;10(2):486-9.
85. Batchelor TT, Sorensen AG, di Tomaso E, Zhang W-T, Duda DG, Cohen KS, et al. AZD2171, a Pan-VEGF Receptor Tyrosine Kinase Inhibitor, Normalizes Tumor Vasculature and Alleviates Edema in Glioblastoma Patients. Cancer cell. 2007;11(1):83-95.
86. Maeda A, Leung MKK, Conroy L, Chen Y, Bu J, Lindsay PE, et al. <italic>In Vivo</italic> Optical Imaging of Tumor and Microvascular Response to Ionizing Radiation. PloS one. 2012;7(8):e42133.
87. Daniel RA, Fisher M, Flores-Merino MV, Battaglia G, Ryan AJ, Blakey DC, et al. Effects of the isoforms of the angiogenic growth factor VEGF on neo-vascularization and tumor response to the tyrosine kinase inhibitor cediranib. Cancer Research. 2011;71(8 Supplement):3279-.
88. Jiang Y, Allen D, Kersemans V, Devery AM, Bokobza SM, Smart S, et al. Acute vascular response to cediranib treatment in human non-small-cell lung cancer xenografts with different tumour stromal architecture. Lung Cancer. 2015;90(2):191-8.
89. Burrell JS, Walker-Samuel S, Baker LC, Boult JK, Jamin Y, Ryan AJ, et al. Evaluation of novel combined carbogen USPIO (CUSPIO) imaging biomarkers in assessing the antiangiogenic effects of cediranib (AZD2171) in rat C6 gliomas. International journal of cancer Journal international du cancer. 2012;131(8):1854-62.
90. Vajkoczy P, Ullrich A, Menger MD. Intravital fluorescence videomicroscopy to study tumor angiogenesis and microcirculation. Neoplasia (New York, NY). 2000;2(1-2):53-61.
91. Yuan F, Salehi HA, Boucher Y, Vasthare US, Tuma RF, Jain RK. Vascular permeability and microcirculation of gliomas and mammary carcinomas transplanted in rat and mouse cranial windows. Cancer Res. 1994;54(17):4564-8.
92. Biel NM, Lee JA, Sorg BS, Siemann DW. Limitations of the dorsal skinfold window chamber model in evaluating anti-angiogenic therapy during early phase of angiogenesis. Vascular Cell. 2014;6:17-.
93. Willett CG, Boucher Y, di Tomaso E, Duda DG, Munn LL, Tong RT, et al. Direct evidence that the VEGF-specific antibody bevacizumab has antivascular effects in human rectal cancer. Nat Med. 2004;10(2):145-7.
94. Batchelor TT, Gerstner ER, Emblem KE, Duda DG, Kalpathy-Cramer J, Snuderl M, et al. Improved tumor oxygenation and survival in glioblastoma patients who show increased blood perfusion after cediranib and chemoradiation. Proc Natl Acad Sci U S A. 2013;110(47):19059-64.

95. Emblem KE, Mouridsen K, Bjornerud A, Farrar CT, Jennings D, Borra RJ, et al. Vessel architectural imaging identifies cancer patient responders to anti-angiogenic therapy. Nat Med. 2013;19(9):1178-83.
96. Sorensen AG, Emblem KE, Polaskova P, Jennings D, Kim H, Ancukiewicz M, et al. Increased survival of glioblastoma patients who respond to antiangiogenic therapy with elevated blood perfusion. Cancer Res. 2012;72(2):402-7.
97. Jain RK. ANTIANGIOGENESIS STRATEGIES REVISITED: FROM STARVING TUMORS TO ALLEVIATING HYPOXIA. Cancer cell. 2014;26(5):605-22.
98. LTD. X. SMALL ANIMAL RADIATION RESEARCH PLATFORM (SARRP). 2016.
99. Maeda A, DaCosta RS. Optimization of the dorsal skinfold window chamber model and multi-parametric characterization of tumor-associated vasculature. IntraVital. 2014;3(1):e27935.
100. Francia G, Cruz-Munoz W, Man S, Xu P, Kerbel RS. Mouse models of advanced spontaneous metastasis for experimental therapeutics. Nat Rev Cancer. 2011;11(2):135-41.
101. Chung AS, Kowanetz M, Wu X, Zhuang G, Ngu H, Finkle D, et al. Differential drug class-specific metastatic effects following treatment with a panel of angiogenesis inhibitors. J Pathol. 2012;227(4):404-16.
102. Huang Y, Goel S, Duda DG, Fukumura D, Jain RK. Vascular normalization as an emerging strategy to enhance cancer immunotherapy. Cancer Res. 2013;73(10):2943-8.
103. Faruque LI, Lin M, Battistella M, Wiebe N, Reiman T, Hemmelgarn B, et al. Systematic Review of the Risk of Adverse Outcomes Associated with Vascular Endothelial Growth Factor Inhibitors for the Treatment of Cancer. PloS one. 2014;9(7):e101145.

ADDENDUM 1

Additional risk and protective factors for CRC development		
Risk Factor	**Level**	**RR (95% CI)**
BMI	30 vs 22 kg/m²	1.10 (1.08-1.12)
Smoking	5 vs. 0 pack-years	1.06 (1.03-1.08)
	30 vs. 0 pack-years	1.26 (1.17-1.36)
Alcohol	5 vs. 0 drinks/wk	1.06 (0.91-1.23)
	30 vs. 0 drinks/wk	1.26 (0.68-2.32)
CRC Family History	Yes vs. No	1.80 (1.61-2.02)
IBD	Yes vs. No	2.93 (1.79-4.81)
Processed Meat	5 vs. 0 servings/wk	1.09 (0.93-1.25)
Red Meat	5 vs. 0 servings/wk	1.13 (1.09-1.16)
Protective Factors	**Level**	**RR (95% CI)**
Physical Activity	An increase of 2 in standardized PA score	0.88 (0.86-0.91)
HT (current)	5 vs. 0 year	0.65 (0.26-1.68)
	10 vs. 0 year	0.61 (0.10-3.96)
HT (former)	5 vs. 0 year	0.96 (0.91-1.02)
	10 vs. 0 year	0.84 (0.70-1.02)
Aspirin/NSAIDs	5 vs. 0 year	0.76 (0.50-1.15)
Fruit	3 vs. 0 serving/d	0.84 (0.75-0.96)
Vegetables	5 vs. 0 servings/d	0.86 (0.78-0.94)

Table 2 (HT= post-menopausal hormone therapy)

Primary CRC prevention
Reduce your risk of colorectal cancer. 1. Get *screened* regularly. 2. Maintain a *healthy weight* throughout life. 3. Adopt a *physically active* lifestyle. 4. Consume a healthy diet with an emphasis on *plant sources*; specifically: *Choose foods and beverages in amounts that help achieve and maintain a healthy weight. Limit consumption of red and processed meat.* *Eat at least 2½ cups of vegetables and fruits each day.* *Choose whole grains instead of refined grain products.* 5. If you drink *alcoholic beverages*, limit consumption. 6. Consume the recommended levels of *calcium*, primarily through food sources 7. *Avoid tobacco* products.

Table 3

Angiogenesis phases physiological and tumorigenic		
Sprouting	**Resolution**	**Fusion**
1. Localized high VEGFA concentrates induce the formation of a vascular stalk by trailing endothelial cell proliferation. The stalk tip cells that breach the basement membrane are exposed to ECM and adopt a proteolytic phenotype for ECM breakdown by MT1-MMP's expression. 2. Lumen formation in the vascular stalk by fusion of endothelial cell vacuoles (44)	Physiologic: 1. VEGF induces Delta-like–ligand 4 (DLL4) expression in EC, attenuating excess angiogenesis through 'communicating' to Notch 1 and 4 receptors on adjacent endothelial cells 2. PDGF-BB production of EC attract pericytes and vascular smooth muscle cells (VSMC). Pericytes and VSMC express Ang1, exerting EC stabilization 3. EC-pericyte contact induces Tissue Inhibition of Metalloproteinase 1 and 2 (TIMP1 and TIMP2), switching of the proteolytic phenotype	Physiologic 1. Proteolytic breakdown of the basement membrane of adjacent vessels by vascular stalk tip 2. VEGF-switch is turned off at sufficient O2 sensitization. HIF is degraded by oxygen dependent proteasome activity (40)
	Tumorigenic: 1. DLL4 signaling is inhibited 2. HIF-1 induces Ang2 upregulation, facilitating antagonist effects to Ang1 (no formation of tight and adherens junctions + deprivation of a basement membrane = leaky vessel constitution). In addition Ang2 chemoattracts TIE-2 expressing monocytes (TEM). TEM are responsible for a	Tumorigenic: VEFG-switch is constitutionally turned on, prohibiting angiogenic resolution and fusion

	supplemental pro-angiogenic factor excretion 3. HIF-1 induced PlGF: facilitation of VEGF R effects (44)	

Table 10

Angiogenesis drives and effect routes		
Drive	**Mechanism activation**	**Effects routes**
-Hypoxia(39) -Stroma NO decline -Reactive Oxidative Species (40-42) -Irradiation (40)	HIF-1 transcription factor increase by inhibiting the HIF-1 proteasome or dissolving hypoxic-stress dependable mRNA molecules from HIF-1 by irradiation	HIF transcription of VEGFA and VEGFR2, angiopoietine 2(AP2), platelet derived growth factor (PDGF), placenta growth factor (PlGF), transforming growth factor α (TGFα), interleukin 8 (IL-8), and hepatocyte growth factor upregulation
Acidosis (43)	RAS-activation and ERK1/2 complex activation, stimulating acidic transcription factor AP-1	Activation of VEGF promotor region: VEGF production and IL8
Tumor PDGFc (platelet derived growth factor) secretion (44)	Consecutive pathways in Tumor Activated Fibroblasts (TAF)	VEGFA, FGF (fibroblast growth factor) (promoting proliferation, migration and differentiation of vascular endothelial cells) and CXCL12 (a molecule recruiting EC from the bone marrow).
Tumor CSF-1 (colony stimulating factor) secretion (44)	Consecutive pathways in Tumor Activated Macrophages or Monocytes (TAM)	*Initiation* of the angiogenic process by upregulation of HIF1 and HIF2 MMP9 (matrix metalloprotease) secretion: remodeling ECM and liberating ECM associated VEGFA
Tumor SCF (stem cell factor) secretion, chemotactically localizing mast cells in the periphery (44)	Consecutive pathways in Mast cells	Production of pro-angiogenic factors: VEGF, IL8, FGF2, TGFβ, TNFα and promote MMP9
Tumor VEGF and GCSF (granulocyte	Consecutive pathways in Myeloid	GCSF, attracting more $CD11b^{+}$Grl cells (continuous immune cell supply), and BV-8, *independently*

colony stimulating factor) secretion (44)	derived suppressor cells ($CD11b^{+}Grl$ cells)	inducing EC proliferation and migration
Tumor GCSF and CXC chemokines secretion (44)	Consecutive pathways in Neutrophils	Polarized into a pro-tumor state under the influence of tumor secreted TGFβ1, they secrete MMP9, VEGFA
Set of mutations in advanced tumors (e.g. HER-2, RAS and V-Src) (45)	Tumor hypoxic mimicry	HIF-1 increase, upregulation of angiogenic oncoproteins (e.g. MAPK,PI3K)
Circulating cytokines (45)		TNFα, IL1β, EGF (epidermal growth factor) and IGF-1 (insulin-like growth factor) are found to enhance HIF activity

Table 11

Treatment resistance in tumors following aberrant angiogeneses		
Microvascular deformity	**Physiologic changes**	**Impaired non-operative treatment**
Spatially and temporally heterogeneous blood supply (37, 50)	Compromising uniform oxygenation and metabolite delivery	-Oxidative based therapies (radiotherapy and some cytotoxic drugs) -Chemotherapy/biologic agents
Vessel wall fenestration malformation(50, 51)	Compromising permselectivity .	-Chemotherapy/biologic agents
Raised Interstitial Fluid Pressure(50)	Compromising extravasation	-Chemotherapy/biologic agents
Deranged tumor cell membrane pH gradient (50)	Compromising mild basic metabolite extravasation	-Chemotherapy/biologic agents
Dysfunctional endothelial signaling (50)	Compromising essential adhesion molecules: ICAM, VCAM and e-selectin	-Immunological treatment and response

Table 12

Microscopes for in vivo imaging		
Microscope	**Image generation**	**Specifications**
Conventional light microscopy (50)	Light reflection and absorption	Relatively high resolution, no penetration depth
Fluorescence laser microscopy (50)	Registers only fluorescence or phosphorescence probes	High resolution (better in confocal fluorescence microscopes), penetration depth up to 100µm (even more and 3D possibilities in multiphoton fluorescence microscopes).
Optical Frequency Domain Reflectometry (OFDR) (55)(50)	Computes interference signals as functions of wavelength resulting between scattered light and reference beams	High resolution, capability of volumetric imaging, also 3D IVM imaging is possible

Table 13

Molecular pathways inhibition of angiogenesis		
Target	*Agent*	*Compound*
VEGF	Anti-VEGF Antibodies	Bevacizumab
VEGFA and PlGF	Antibody mimicking VEGFR1 and VEGFR2 on the Fc domain (VEGF and PlGF trap)	Aflibercept
Ligand binding site of various RTK's (receptor tyrosine kinases) ATP binding site of various (e.g. VEGF) RTK's	Small molecule RTK inhibitors	Cediranib and many others
EGF (epidermal growth factor)-RTK's	Non-small molecule RTK inhibitors.	Cetuximab and panitumumab
HIF upregulation	Inhibitors of PI3/ATK/mTOR pathway	LY294002 and wortmannin/ FARA-A/ Rapamycin, Tensirolimus and Everolimus
HIF upregulation	Inhibitors MAPK-Farnesyltransferase Rho and Ras	Tipifarnib and Lonafarnib

HIF cascade	Molecular inhibition of the HIF DNA target sequence (HRE)	No successful compound yet
HIF and oncoproteins folding	Inhibition of chaperone molecule (Heat shock protein 90)	
HIF upregulation		Thioredoxin
Targeting EC proliferation and migration		
Sprouting (58)	Inhibition of ECM breakdown	Marimistat and Neovastat
Tubulin polymerization	Cell cycle arrest agent in endothelial cells	2-methoxyestradiol (2ME2)
Stromal cell activation inhibition		
Interruption of BV-8-GCSF-mechanism	Independently block tumor angiogenesis	
Indirect Endogenous inhibitors		
IFNα	Inhibition of bFGF and VEGF production (possible use of TEM as cellular vehicle)	
Direct Endogenous inhibitors		
Thrombospondin 1, Endostatin, Tumstatin, Canstatin, Arrestin and others	These substances directly bind to adhesion molecules (CAM) expressed on the surface of actively proliferating endothelial cells. They facilitate apoptosis and/or inhibition of migrating and/or proliferating cells	
Elusive inhibition		
Lodamin (TNP470)	Tumor growth and angiogenesis arrest	
Thalidomide	Exerts anti-angiogenic effects	

Table 14

ADDENDUM 2

Protocol Dorsal Skinfold Window Chamber Implantation Technique

Materials

1. Inhalation anesthesia (Isoflurane, 5% induction, 2% maintenance)
2. Window chamber parts (2 chambers, 1 window, 3 screws, 4 bolts, 1 tension ring)
3. Wrench and tension ring tongs
4. Cup with ethanol (large enough to fit all the instruments)
5. Sterile :
    a. Needle holder
    b. Pincet
    c. Scalpel
    d. Fine scissors
    e. Micropincet
    f. Microscissors
6. Heated tableau
7. Physiologic water
8. Eye-creme containing antibiotics
9. 3/0 vycril thread to suspend the skinfold
10. 6/0 thread mono PDSII
11. Infra-red lamp

Method

1. Inhalation anesthesia (Isoflurane, 5% induction, 2% maintenance)
2. Transfer animal to the heated pad on operation table
3. Suspend the skinfold with two vycril threads on locations (illustrated in the figure below) to a horizontal tube (here: lightning tube) using two kochers.
4.  -> Pay attention to suspend the skin sufficiently for an operable stretch
5. Prepare one window chamber half with three screws (upper screw : two bolts on each side of chamber; two lower screws: only 1 bolt)
6. Use non-absorbable thread 6/0, to sew in the window chamber, thus penetrating the skinfold on 7 locations with 5 surgical nods at each hole
7. Pierce the skinfold with the scalpel at the locations of the two lower screws and check the opening width with a pink 18G needle (avoid blood vessels and make sure to penetrate each fascia accurately to reduce pain and dap bleeding if necessary)

8. Use light to transilluminate the chamber, and demarcate the circle of the microscopic field
9. Remove the upper skin overlaying the demarcated circle with the pincet and scissors (whilst humidifying the subcutis with physiologic water)
10. Use a micropincet and microscissors to remove the little fascia of the subcutis, as such the vasculature of the opposing mucosa is clearly seen (be careful not to affect blood vessels)
11. Apply the second half of the window chamber (tauten the upper bolts well, the lower bolts are more loose)
12. Administer physiologic water to the microscopy field (just enough, no leaking)
13. Apply the cover glass (avoid the formation of air bubbles)
14. Apply the tension ring (VERY carefully)
15. Place the mouse in a cage with a high grid underneath an infra red lamp

Protocol Capimage Analyses

Capimage is a software product of German craft. Its use is confined by its properties to quickly analyse microvasculature parameters. In this protocol the use for microvasculature density, blood vessel length, area fraction, red blood cell velocity, diameter, volumetric velocity and tortuosity are explained step by step.

Interpretation of data is contextual.

Scale setting

1. Generate a prototype image with scale bar
2. Run Capimage
3. First window: press ‘open’
4. Press ‘file’ in the left upper corner
5. In the roll out screen, press ‘image file open’
6. Open the prototype image
7. In the upper bar press options
8. In the roll out screen select ‘magnification ascertation’
9. Draw a line horizontal over the scale bar precisely from end to end, use a ruler to measure the ‘horizontal distance at screen’.
10. Draw a vertical line with exactly the same distance at screen
11. The input screen opens, fill in the ‘horizontal distance at screen’, followed by the true horizontal distance displayed by the scale bar and the true vertical distance (same as true horizontal)
12. Press ‘calculate’
13. Press ‘Save into’, select a nr from 1-6
14. Back in the main window: select in the second bar ‘magn’ the 1-6 nr.

Blood vessel density

1. Run Capimage
2. First window: press ‘open’
3. Press ‘file’ in the left upper corner
4. In the roll out screen, press ‘video file open’

5. Grab your video (anticipate your choice of video to optimize your outcomes)
6. Open
7. Press ‘DensNA’ in the second bar and press ‘bigwindow’ to make sure you include the full window
8. Now start counting the vessels -at every branch a new vessel starts- by marking them systematically with a left mouse click, first mark the biggest vessels, further on the small ones
9. Tip: Adjust contrast/brightness: in the menu ‘options’, select ‘contrast’. Adjust by moving the pointer under ‘display’
10. Tip: press live to play the video, thus vessels are better visualized. By typing 1 in the search section and pressing live again you repeat the video. Once the video shows you a clear vision, it’s optional to stop the video and further analyze the frozen image.
11. Removing a marker: right click on the marker
12. To command a counting: put a right click on the screen. The counting will be shown in the table on the right, you can now simply copy the result into an excel file (copy+paste).
13. By pressing clear in the third bar, you remove the red markers to start a new video. To clear the table, press ‘clear table’.
14. Estimated time per video: 4 mins

Blood vessel length

1. Run Capimage
2. First window: press ‘open’
3. Press ‘file’ in the left upper corner
4. In the roll out screen, press ‘video file open’
5. Grab your video (anticipate your choice of video to optimize your outcomes)
6. Open
7. Press ‘DensLA’ in the second bar and press ‘bigwindow’ to make sure you include the full window
8. Draw a line holding a left mouse click for each and every vessel. After finishing, right mouse click on the screen. The measurement appears in the table on the right. Simply copy+paste into excell.
9. Tip: Adjust contrast/brightness: in the menu ‘options’, select ‘contrast’. Adjust by moving the pointer under ‘display’
10. Tip: press live to play the video, thus vessels are better visualized. By typing 1 in the search section and pressing live again you can repeat the video. Once the video shows you a clear vision, it’s optional to stop the video and further analyze the frozen image.
11. Removing a line: click ‘erase line’ in the third bar. The last drawn line will be erased.
12. By pressing clear in the third bar, you remove the red lines to start a new video. To clear the table, press ‘clear table’.
13. Estimated time per video: 7 mins

Red blood cell velocity, diameter and volumetric velocity

1. Run Capimage
2. First window: press ‘open’
3. Press ‘file’ in the left upper corner

4. In the roll out screen, press ‘video file open’
5. Grab your video (anticipate your choice of video to optimize your outcomes)
6. Open
7. Press ‘DiamMa’
8. Select 9 prominent vessels, draw a line using 2 left clicks along each diameter of every vessel
9. Diameters appear in the table on the right
10. Go to ‘file’ select ‘save table into excell’
11. A new excel file opens, cancel saving the new file
12. Rewrite values in another column without the litteral characters (like D, and micro meter…)
13. Copy the column into your excel file and calculate the average value of the 9 diameters.
14. The measure of the red blood cell velocity is done right after a set of 9 diameters is measured
15. Remember the exact location of the former 9 measurements for diameter
16. Select veloLSD and draw a line along the same 9 diameters in the same sequence using two right clicks.
17. Now reset the video in search to ‘1’ and press ‘live’, immediately followed by RunLSD
18. Now Capimage is measuring the red blood cell velocity in each vessel. Wait until completing.
19. A new screen appears, showing 9 bars.
20. Each bar stands for a chronical display of contrast velocity in each vessel over time.
21. IMPORTANT: select in the table on the right: ‘detail values’
22. Now randomly 4 left clicks along the first bar and finish by pressing in the table on the right: ‘standard table’
23. Now you have a mean value of the velocity of the first vessel
24. Repeat the same procedure for the remaining 8 vessels
25. When done, go to ‘file’, select ‘save into excell’
26. A new excel file opens, cancel saving the new file
27. Rewrite values in another column without the litteral characters (like mean, etc…)
28. Copy the column into your excel file and calculate the average value of the 9 velocities.
29. Time estimated per video: 9 mins

Protocol ImageJ Analyses

Scale setting

1. Run ImageJ
2. File, Open, and open the prototype image with scale bar
3. Select the pictogram to draw a Straight line and draw a straight line that covers the scale bar
    a. Analyze, Set scale…
    b. Known distance: 100µm (length of the scale bar)
    c. Unit of length: µm

d. Select Global
e. OK

Tortuosity

1. Run ImageJ
2. Set scale (see topic Scale setting)
3. File, Open, and open the image you want to analyze
4. Select the pictogram to draw a Straight line, right mouse click and select Segmented line
5. Choose a random vessel crossing an imaginary vertical line in the middle of the image
6. Draw with the Segmented line tool a line following the vessel wall of one vessel segment (= part of the vessel between two bifurcations); to end the line: right mouse click
7. Analyze, Measure. This distance represents the length of the segment following the vessel wall (=L)
8. Then draw a line that measures the shortest distance of the segment (a straight line from the start of the segment to the end of the segment)
9. Analyze, Measure. This distance represents the shortest distance from the start of the segment to the end of the segment (=SP)
10. Copy the results into an Excell file and calculate the tortuosity index with the following formula: Tortuosity= (1-SP/L)*100

Measure 10 vessel per image, 3 locations per mouse.

Measure videos before and after treatment.

Permeability

1. Run ImageJ
2. Set scale (see topic Scale setting)
3. Set measurements: Analyze, Set measurements, select Area and Mean gray value
4. Open ROI manager: Analyze, Tools, ROI manager
5. File, Open, and open the video you want to analyze
6. Select the pictogram to draw a Freehand selections
7. Choose a random area in the interstitium and delineate this area with the Freehand selection tool
8. Add the ROI to the ROI manager by pressing Add in the ROI manager
9. Delineate 10 random interstitial ROI and add them to the ROI manager
10. Press Plugins, Time Series Analyzer V3
11. Press Get average in the Time Series Analyzer V3 window
12. A results window will open with all the average grey values per ROI per time frame, and the average grey value of all 10 ROI's per time frame
13. Copy the average of all 10 ROI's per time frame into an Excell file

Measure 4 time points per mouse (all at the same location)

Measure videos before and after treatment.

ADDENDUM 3
MICROVASCULAR DENSITY

DESCRIPTIVES

Descriptive Statistics of Microvascular Density Ratios

	N	Range	Minimum	Maximum	Mean	Std. Deviation
Controls	6	1,38990	,37719	1,76709	,9808370	,52185439
Cediranib	6	,67313	,44290	1,11602	,7618964	,22540117
Radiotherapy	6	,92893	,30195	1,23088	,7366460	,31312980
Concurrent Therapy	6	,61301	,61268	1,22569	,9195994	,20367123
Valid N (listwise)	6					

Tests of Normality for Microvascular Density Ratio Distributions

	Kolmogorov-Smirnov[a]			Shapiro-Wilk		
	Statistic	df	Sig.	Statistic	df	Sig.
Controls	,156	6	,200*	,962	6	,837
Cediranib	,229	6	,200*	,952	6	,760
Radiotherapy	,184	6	,200*	,980	6	,950
Concurrent Therapy	,195	6	,200*	,969	6	,886

*. This is a lower bound of the true significance.

a. Lilliefors Significance Correction

INDUCTIVES

KRUSKAL-WALLIS ONE WAY ANALYSIS OF VARIANCE ON RANKS WOENSDAG, APRIL 06, 2016, 18:46:23

Data source: Data 1 in Notebook1

Normality Test (Shapiro-Wilk): Passed (P = 0,702)

Equal Variance Test (Brown-Forsythe): Passed (P = 0,132)

Group N Missing Median 25% 75%

Col 1	6	0	0,903	0,506	1,481
Col 2	6	0	0,789	0,571	0,895
Col 3	6	0	0,747	0,477	0,951
Col 4	6	0	0,904	0,783	1,080

H = 2,607 with 3 degrees of freedom. (P = 0,456)

The differences in the median values among the treatment groups are not great enough to exclude the possibility that the difference is due to random sampling variability; there is not a statistically significant difference (P = 0,456)

MANN-WHITNEY RANK SUM TEST CONTROLS GROUP VS. CONCURRENT MODALITY TREATMENT GROUP WOENSDAG, APRIL 06, 2016, 18:50:14

Data source: Data 1 in Notebook1

Normality Test (Shapiro-Wilk): Passed (P = 0,949)

Equal Variance Test: Passed (P = 0,072)

Group	**N**	**Missing**	**Median**	**25%**	**75%**
Col 1	6	0	0,903	0,506	1,481
Col 4	6	0	0,904	0,783	1,080

Mann-Whitney U Statistic= 17,000

T = 38,000 n(small)= 6 n(big)= 6 P(est.)= 0,936 P(exact)= 0,937

The difference in the median values between the two groups is not great enough to exclude the possibility that the difference is due to random sampling variability; there is not a statistically significant difference (P = 0,937)

MICROVASCULAR LENGTH

DESCRIPTIVES

Descriptive Statistics

	N	Range	Minimum	Maximum	Mean	Std. Deviation
LengthControls	6	,60999	,39635	1,00634	,6945356	,22084394
LengthCediranib	6	,61539	,37206	,98745	,7150473	,19876505
LengthRadiotherapy	6	,22260	,53633	,75893	,6315200	,09847671
LengthConcurrent	6	,72652	,73016	1,45668	1,0107661	,24136882
Valid N (listwise)	6					

Tests of Normality

	Kolmogorov-Smirnov[a]			Shapiro-Wilk		
	Statistic	df	Sig.	Statistic	df	Sig.
LengthControls	,143	6	,200*	,982	6	,960
LengthCediranib	,254	6	,200*	,889	6	,312
LengthRadiotherapy	,292	6	,120	,847	6	,149
LengthConcurrent	,329	6	,041	,860	6	,189

*. This is a lower bound of the true significance.

a. Lilliefors Significance Correction

INDUCTIVES

KRUSKAL-WALLIS ONE WAY ANALYSIS OF VARIANCE ON RANKS WOENSDAG, APRIL 06, 2016, 18:55:42

Data source: Data 1 in Notebook1

Normality Test (Shapiro-Wilk): Passed (P = 0,480)

Equal Variance Test (Brown-Forsythe): Passed (P = 0,759)

Group	N	Missing	Median	25%	75%
Col 1	6	0	0,718	0,476	0,871
Col 2	6	0	0,749	0,599	0,815

Col 3	6	0	0,610	0,546	0,733
Col 4	6	0	0,980	0,861	1,124

H = 8,367 with 3 degrees of freedom. (P = 0,039)

The differences in the median values among the treatment groups are greater than would be expected by chance; there is a statistically significant difference (P = 0,039)

To isolate the group or groups that differ from the others use a multiple comparison procedure.

All Pairwise Multiple Comparison Procedures (Dunn's Method) :

Comparison	**Diff of Ranks**		**Q**	**P**	**P<0,050**
Col 4 vs Col 3	11,333	2,776	0,033	Yes	
Col 4 vs Col 1	8,167	2,000	0,273	No	
Col 4 vs Col 2	7,833	1,919	0,330	Do Not Test	
Col 2 vs Col 3	3,500	0,857	1,000	No	
Col 2 vs Col 1	0,333	0,0816	1,000	Do Not Test	
Col 1 vs Col 3	3,167	0,776	1,000	Do Not Test	

Note: The multiple comparisons on ranks do not include an adjustment for ties.

MICROVASCULAR DIAMETER

DESCRIPTIVES

Descriptive Statistics

	N	Range	Minimum	Maximum	Mean	Std. Deviation
DiameterControls	6	,88917	1,12901	2,01818	1,5538278	,34977242
DiameterCediranib	6	,92832	1,05586	1,98418	1,3282880	,33385531
DiameterRadiotherapy	6	,47620	1,19370	1,66990	1,4251471	,17774869
DiameterConcurrent	6	,72470	1,00000	1,72470	1,2906395	,27612809
Valid N (listwise)	6					

Tests of Normality

	Kolmogorov-Smirnov[a]			Shapiro-Wilk		
	Statistic	df	Sig.	Statistic	df	Sig.
DiameterControls	,203	6	,200*	,939	6	,652
DiameterCediranib	,337	6	,031	,755	6	,022
DiameterRadiotherapy	,215	6	,200*	,948	6	,721
DiameterConcurrent	,208	6	,200*	,930	6	,580

*. This is a lower bound of the true significance.

a. Lilliefors Significance Correction

INDUCTIVES

KRUSKAL-WALLIS ONE WAY ANALYSIS OF VARIANCE ON RANKS WOENSDAG, APRIL 06, 2016, 19:04:21

Data source: Data 1 in Notebook1

Normality Test (Shapiro-Wilk): Passed (P = 0,258)

Equal Variance Test (Brown-Forsythe): Passed (P = 0,508)

Group	N	Missing	Median	25%	75%
Col 1	6	0	1,571	1,211	1,851

Col 2	6	0	1,229	1,124	1,490
Col 3	6	0	1,421	1,280	1,570
Col 4	6	0	1,259	1,043	1,514

H = 3,247 with 3 degrees of freedom. (P = 0,355)

The differences in the median values among the treatment groups are not great enough to exclude the possibility that the difference is due to random sampling variability; there is not a statistically significant difference (P = 0,355)

MANN-WHITNEY RANK SUM TEST CEDIRANIB VS CONTROLS GROUP WOENSDAG, APRIL 06, 2016, 19:07:11

Data source: Data 1 in Notebook1

Normality Test (Shapiro-Wilk): Passed (P = 0,411)

Equal Variance Test: Passed (P = 0,409)

Group	**N**	**Missing**	**Median**	**25%**	**75%**
Col 1	6	0	1,571	1,211	1,851
Col 2	6	0	1,229	1,124	1,490

Mann-Whitney U Statistic= 10,000

T = 47,000 n(small)= 6 n(big)= 6 P(est.)= 0,230 P(exact)= 0,240

The difference in the median values between the two groups is not great enough to exclude the possibility that the difference is due to random sampling variability; there is not a statistically significant difference (P = 0,240)

MANN-WHITNEY RANK SUM TEST CONTROLS GROUP VS. CONCURRENT MODALITY TREATMENT GROUP WOENSDAG, APRIL 06, 2016, 19:10:02

Data source: Data 1 in Notebook1

Normality Test (Shapiro-Wilk): Passed (P = 0,423)

Equal Variance Test: Passed (P = 0,354)

Group	**N**	**Missing**	**Median**	**25%**	**75%**
Col 1	6	0	1,571	1,211	1,851
Col 4	6	0	1,259	1,043	1,514

Mann-Whitney U Statistic= 9,000

T = 48,000 n(small)= 6 n(big)= 6 P(est.)= 0,173 P(exact)= 0,180

The difference in the median values between the two groups is not great enough to exclude the possibility that the difference is due to random sampling variability; there is not a statistically significant difference (P = 0,180)

CENTERLINE RED BLOOD CELL VELOCITY

DESCRIPTIVES

Descriptive Statistics

	N	Range	Minimum	Maximum	Mean	Std. Deviation
RBCVContrils	6	,91521	,73045	1,64566	1,1963792	,29339071
RBCVCediranib	6	,64306	,96030	1,60336	1,2003329	,22547632
RBCVRadiotherapy	6	,65048	1,05283	1,70332	1,3111688	,28358275
RBCVConcurrent	6	,84271	,93397	1,77667	1,3993938	,33805727
Valid N (listwise)	6					

Tests of Normality

	Kolmogorov-Smirnov[a]			Shapiro-Wilk		
	Statistic	df	Sig.	Statistic	df	Sig.
RBCVContrils	,254	6	,200*	,929	6	,573
RBCVCediranib	,240	6	,200*	,907	6	,419
RBCVRadiotherapy	,246	6	,200*	,848	6	,152
RBCVConcurrent	,256	6	,200*	,900	6	,376

*. This is a lower bound of the true significance.

a. Lilliefors Significance Correction

INDUCTIVES

KRUSKAL-WALLIS ONE WAY ANALYSIS OF VARIANCE ON RANKS WOENSDAG, APRIL 06, 2016, 19:14:17

Data source: Data 1 in Notebook1

Normality Test (Shapiro-Wilk): Passed (P = 0,465)

Equal Variance Test (Brown-Forsythe): Passed (P = 0,824)

Group	N	Missing	Median	25%	75%
Col 1	6	0	1,195	1,036	1,367

Col 2	6	0	1,145	1,035	1,367
Col 3	6	0	1,210	1,071	1,636
Col 4	6	0	1,496	1,014	1,684

H = 1,067 with 3 degrees of freedom. (P = 0,785)

The differences in the median values among the treatment groups are not great enough to exclude the possibility that the difference is due to random sampling variability; there is not a statistically significant difference (P = 0,785)

MANN-WHITNEY RANK SUM TEST CONTROLS VS CEDIRANIB MONOTHERAPY GROUP WOENSDAG, APRIL 06, 2016, 19:16:41

Data source: Data 1 in Notebook1

Normality Test (Shapiro-Wilk): Passed (P = 0,448)

Equal Variance Test: Passed (P = 0,753)

Group	**N**	**Missing**	**Median**	**25%**	**75%**
Col 1	6	0	1,195	1,036	1,367
Col 2	6	0	1,145	1,035	1,367

Mann-Whitney U Statistic= 15,000

T = 42,000 n(small)= 6 n(big)= 6 P(est.)= 0,689 P(exact)= 0,699

The difference in the median values between the two groups is not great enough to exclude the possibility that the difference is due to random sampling variability; there is not a statistically significant difference (P = 0,699)

MANN-WHITNEY RANK SUM TEST CONTROLS GROUP VS. CONCURRENT MODALITY TREATMENT GROUP WOENSDAG, APRIL 06, 2016, 19:19:30

Data source: Data 1 in Notebook1

Normality Test (Shapiro-Wilk): Passed (P = 0,364)

Equal Variance Test: Passed (P = 0,625)

Group	**N**	**Missing**	**Median**	**25%**	**75%**
Col 1	6	0	1,195	1,036	1,367
Col 4	6	0	1,496	1,014	1,684

Mann-Whitney U Statistic= 12,000

T = 33,000 n(small)= 6 n(big)= 6 P(est.)= 0,378 P(exact)= 0,394

The difference in the median values between the two groups is not great enough to exclude the possibility that the difference is due to random sampling variability; there is not a statistically significant difference (P = 0,394)

VOLUMETRIC BLOOD FLOW

DESCRIPTIVES

Descriptive Statistics

	N	Range	Minimum	Maximum	Mean	Std. Deviation
VQControls	6	5,58323	1,11964	6,70287	3,1933535	2,03346877
VQCediranib	6	5,02067	1,29170	6,31237	2,4011869	1,94577422
VQRadiotherapy	6	3,24962	1,50020	4,74983	2,7365802	1,08238750
VQConcurrent	6	4,35091	,93397	5,28488	2,6041773	1,63130447
Valid N (listwise)	6					

Tests of Normality

	Kolmogorov-Smirnov[a]			Shapiro-Wilk		
	Statistic	df	Sig.	Statistic	df	Sig.
VQControls	,188	6	,200*	,918	6	,490
VQCediranib	,362	6	,014	,637	6	,001
VQRadiotherapy	,322	6	,051	,851	6	,159
VQConcurrent	,163	6	,200*	,933	6	,601

*. This is a lower bound of the true significance.

a. Lilliefors Significance Correction

INDUCTIVES

KRUSKAL-WALLIS ONE WAY ANALYSIS OF VARIANCE ON RANKS ZONDAG, MAART 06, 2016, 13:05:21

Data source: Data 1 in Notebook1

Normality Test (Shapiro-Wilk): Failed (P < 0,050)

Group	N	Missing	Median		25%	75%
Col 1	6	0	2,882	1,499	4,638	
Col 2	6	0	1,554	1,397	3,275	

Col 3	6	0	2,565	2,079	3,262
Col 4	6	0	2,400	1,106	3,904

H = 1,753 with 3 degrees of freedom. (P = 0,625)

The differences in the median values among the treatment groups are not great enough to exclude the possibility that the difference is due to random sampling variability; there is not a statistically significant difference (P = 0,625)

MANN-WHITNEY RANK SUM TEST: CEDIRANIB MONOTHERAPY GROUP VS CONCURRENT MODALITY TREATMENT GROUP ZONDAG, MAART 06, 2016, 13:31:43

Data source: Data 1 in Notebook1

Normality Test (Shapiro-Wilk): Failed (P < 0,050)

Group	**N**	**Missing**	**Median**	**25%**	**75%**
Col 2	6	0	1,554	1,397	3,275
Col 4	6	0	2,400	1,106	3,904

Mann-Whitney U Statistic= 17,000

T = 38,000 n(small)= 6 n(big)= 6 P(est.)= 0,936 P(exact)= 0,937

The difference in the median values between the two groups is not great enough to exclude the possibility that the difference is due to random sampling variability; there is not a statistically significant difference (P = 0,937)

TORTUOSITY INDEX

DESCRIPTIVES

Descriptives

			Statistic	Std. Error
TorqControls	Mean		8,1349712	2,89234450
	95% Confidence Interval for Mean	Lower Bound	,6999630	
		Upper Bound	15,5699794	
	5% Trimmed Mean		7,7952436	
	Median		4,1706837	
	Variance		50,194	
	Std. Deviation		7,08476818	
	Minimum		2,69143	
	Maximum		19,69361	
	Range		17,00218	
	Interquartile Range		12,07915	
	Skewness		1,186	,845
	Kurtosis		-,417	1,741
TorqCediranib	Mean		1,0890512	,20009658
	95% Confidence Interval for Mean	Lower Bound	,5746866	
		Upper Bound	1,6034159	
	5% Trimmed Mean		1,0723829	
	Median		1,0080065	
	Variance		,240	
	Std. Deviation		,49013453	
	Minimum		,60717	
	Maximum		1,87096	
	Range		1,26380	

	Interquartile Range		,91654	
	Skewness		,751	,845
	Kurtosis		-,318	1,741
TorqRadiotherapy	Mean		3,4459435	,66780656
	95% Confidence Interval for Mean	Lower Bound	1,7292920	
		Upper Bound	5,1625949	
	5% Trimmed Mean		3,3677190	
	Median		3,2921357	
	Variance		2,676	
	Std. Deviation		1,63578533	
	Minimum		1,92121	
	Maximum		6,37871	
	Range		4,45750	
	Interquartile Range		2,44000	
	Skewness		1,278	,845
	Kurtosis		1,932	1,741
TorqConcurrent	Mean		3,4552208	1,15461775
	95% Confidence Interval for Mean	Lower Bound	,4871814	
		Upper Bound	6,4232602	
	5% Trimmed Mean		3,4364677	
	Median		2,8770932	
	Variance		7,999	
	Std. Deviation		2,82822433	
	Minimum		,49839	
	Maximum		6,74960	
	Range		6,25121	
	Interquartile Range		5,79011	
	Skewness		,306	,845

Kurtosis	-2,423	1,741

Tests of Normality

	Kolmogorov-Smirnov[a]			Shapiro-Wilk		
	Statistic	df	Sig.	Statistic	df	Sig.
TorqControls	,364	6	,013	,772	6	,032
TorqCediranib	,164	6	,200*	,922	6	,519
TorqRadiotherapy	,253	6	,200*	,876	6	,250
TorqConcurrent	,249	6	,200*	,851	6	,162

*. This is a lower bound of the true significance.

a. Lilliefors Significance Correction

INDUCTIVES

KRUSKAL-WALLIS ONE WAY ANALYSIS OF VARIANCE ON RANKS ZONDAG, MAART 06, 2016, 14:39:37

Data source: Data 1 in Notebook1

Normality Test (Shapiro-Wilk): Failed (P < 0,050)

Group	N	Missing	Median		25%	75%
Col 1	6	0	4,171	3,540	15,619	
Col 2	6	0	1,008	0,617	1,533	
Col 3	6	0	3,292	1,989	4,429	
Col 4	6	0	2,877	0,909	6,699	

H = 10,987 with 3 degrees of freedom. (P = 0,012)

The differences in the median values among the treatment groups are greater than would be expected by chance; there is a statistically significant difference (P = 0,012)

To isolate the group or groups that differ from the others use a multiple comparison procedure.

All Pairwise Multiple Comparison Procedures (Tukey Test):

Comparison	Diff of Ranks	q	P	P<0,050
Col 1 vs Col 2	80,000	4,619	0,006	Yes
Col 1 vs Col 4	36,000	2,078	0,456	No

Col 1 vs Col 3	28,000	1,617	0,663	Do Not Test
Col 3 vs Col 2	52,000	3,002	0,146	No
Col 3 vs Col 4	8,000	0,462	0,988	Do Not Test
Col 4 vs Col 2	44,000	2,540	0,275	Do Not Test

Note: The multiple comparisons on ranks do not include an adjustment for ties.

A result of "Do Not Test" occurs for a comparison when no significant difference is found between the two rank sums that enclose that comparison. For example, if you had four rank sums sorted in order, and found no significant difference between rank sums 4 vs. 2, then you would not test 4 vs. 3 and 3 vs. 2, but still test 4 vs. 1 and 3 vs. 1 (4 vs. 3 and 3 vs. 2 are enclosed by 4 vs. 2: 4 3 2 1). Note that not testing the enclosed rank sums is a procedural rule, and a result of Do Not Test should be treated as if there is no significant difference between the rank sums, even though one may appear to exist.

MANN-WHITNEY RANK SUM TEST: CONTROLS GROUP VS CEDIRANIB MONOTHERAPY GROUP ZONDAG, MAART 06, 2016, 14:48:00

Data source: Data 1 in Notebook1

Normality Test (Shapiro-Wilk): Failed (P < 0,050)

Group	N	Missing	Median	25%	75%
Col 1	6	0	4,171	3,540	15,619
Col 2	6	0	1,008	0,617	1,533

Mann-Whitney U Statistic= 0,000

T = 57,000 n(small)= 6 n(big)= 6 P(est.)= 0,005 P(exact)= 0,002

The difference in the median values between the two groups is greater than would be expected by chance; there is a statistically significant difference (P = 0,002)

MANN-WHITNEY RANK SUM TEST RADIOTHERAPY MONOTHERAPY GROUP VS CONCURRENT MODALITY TREATMENT GROUP WOENSDAG, APRIL 06, 2016, 19:33:40

Data source: Data 1 in Notebook1

Normality Test (Shapiro-Wilk): Passed (P = 0,225)

Equal Variance Test: Passed (P = 0,076)

Group	N	Missing	Median	25%	75%
Col 3	6	0	3,292	1,989	4,429
Col 4	6	0	2,877	0,909	6,699

Mann-Whitney U Statistic= 17,000

T = 40,000 n(small)= 6 n(big)= 6 P(est.)= 0,936 P(exact)= 0,937

The difference in the median values between the two groups is not great enough to exclude the possibility that the difference is due to random sampling variability; there is not a statistically significant difference (P = 0,937)

Permeability Index

Descriptives

Inductives Regression function 0’’-30’’

	Control	Cediranib	Radiotherapy	Combination	Global (shared)
Comparison of Fits					
Null hypothesis					One curve for all data sets
Alternative hypothesis					Different curve for each data set
P value					**< 0.0001**
Conclusion (alpha = 0.05)					Reject null hypothesis
Preferred model					Different curve for each data set
F (DFn, DFd)					373.4 (9,11724)
Different curve for each data set					
Best-fit values					
Y0	-1,635	-10,24	-1,915	-6,393	
Plateau	166,9	150,5	124,9	134,6	
K	0,04989	0,0409	0,05747	0,03656	
Tau	20,05	24,45	17,4	27,35	
Half-time	13,89	16,95	12,06	18,96	
Span	168,5	160,7	126,8	141	
Std. Error					
Y0	1,134	1,046	2,109	0,7153	
Plateau	5,256	7,286	7,325	6,276	
K	0,002838	0,003064	0,006565	0,002559	
Span	4,622	6,651	6,25	5,826	
95% Confidence Intervals					
Y0	-3.857 to 0.5872	-12.29 to -8.190	-6.050 to 2.219	-7.795 to -4.991	
Plateau	156.6 to 177.2	136.2 to 164.8	110.5 to 139.2	122.3 to 146.9	
K	0.04432 to 0.05545	0.03489 to 0.04690	0.04460 to 0.07034	0.03154 to 0.04157	
Tau	18.03 to 22.56	21.32 to 28.66	14.22 to 22.42	24.05 to 31.70	
Half-time	12.50 to 15.64	14.78 to 19.87	9.855 to 15.54	16.67 to 21.98	
Span	159.5 to 177.6	147.7 to 173.8	114.5 to 139.0	129.6 to 152.4	
Hougaard's Measure of Skewness					
Y0	-0,0167	-0,0184	-0,03795	-0,01552	
Plateau	0,3213	0,4319	0,6314	0,4069	
K	0,01351	0,01217	0,03536	0,009155	
Goodness of Fit					
Degrees of Freedom	2931	2931	2931	2931	
R square	0,796	0,7654	0,428	0,8223	
Adjusted R square	0,7959	0,7652	0,4277	0,8222	
Absolute Sum of Squares	935536	835764	3110000	400404	Sum: 5281704
Sy.x	17,87	16,89	32,58	11,69	
Normality of Residuals					
D'Agostino & Pearson omnibus K2	133,3	195,3	365,4	859,6	
P value	< 0.0001	< 0.0001	< 0.0001	< 0.0001	
Shapiro-Wilk W	0,9513	0,9429	0,8971	0,8836	
P value	< 0.0001	< 0.0001	< 0.0001	< 0.0001	
Kolmogorov-Smirnov distance	0,09378	0,1232	0,1504	0,1275	
P value	< 0.0001	< 0.0001	< 0.0001	< 0.0001	
Replicates test for lack of fit					
SD replicates	19,43	18,18	35,57	12,34	
SD lack of fit	5,018	7,514	5,88	7,584	
Discrepancy (F)	0,06669	0,1708	0,02732	0,3776	
P value	1	1	1	1	
Evidence of inadequate model?	No	No	No	No	
Covariance Matrix					
Y0 & Plateau	0,6332	0,6531	0,6163	0,6628	
Y0 & K	-0,7295	-0,7323	-0,7271	-0,7337	
Plateau & K	-0,9841	-0,9896	-0,9784	-0,9917	
Dependency					
Y0	0,7592	0,7825	0,7403	0,794	
Plateau	0,9837	0,9902	0,9764	0,9927	
K	0,9873	0,9921	0,9821	0,994	
Constraints					
K	K > 0.0	K > 0.0	K > 0.0	K > 0.0	
One curve for all data sets					
Best-fit values					
Y0	-4,909	-4,909	-4,909	-4,909	-4,909
Plateau	142,6	142,6	142,6	142,6	142,6
K	0,04612	0,04612	0,04612	0,04612	0,04612
Tau	21,68	21,68	21,68	21,68	21,68
Half-time	15,03	15,03	15,03	15,03	15,03
Span	147,5	147,5	147,5	147,5	147,5
Std. Error					

Y0		0,7559	0,7559	0,7559	0,7559	0,7559
Plateau		4,115	4,115	4,115	4,115	4,115
K		0,002254	0,002254	0,002254	0,002254	0,002254
Span		3,676	3,676	3,676	3,676	3,676
95% Confidence Intervals						
Y0	-6.390 to -3.427	-6.390 to -3.427	-6.390 to -3.427	-6.390 to -3.427	-6.390 to -3.427	
Plateau	134.5 to 150.7	134.5 to 150.7	134.5 to 150.7	134.5 to 150.7	134.5 to 150.7	
K	0.04170 to 0.05054	0.04170 to 0.05054	0.04170 to 0.05054	0.04170 to 0.05054	0.04170 to 0.05054	
Tau	19.79 to 23.98	19.79 to 23.98	19.79 to 23.98	19.79 to 23.98	19.79 to 23.98	
Half-time	13.72 to 16.62	13.72 to 16.62	13.72 to 16.62	13.72 to 16.62	13.72 to 16.62	
Span	140.3 to 154.7	140.3 to 154.7	140.3 to 154.7	140.3 to 154.7	140.3 to 154.7	
Hougaard's Measure of Skewness						
Y0		-0,01338	-0,01338	-0,01338	-0,01338	-0,01338
Plateau		0,2785	0,2785	0,2785	0,2785	0,2785
K		0,009996	0,009996	0,009996	0,009996	0,009996
Goodness of Fit						
Degrees of Freedom						11733
R square		0,6138	0,7432	0,4232	0,5683	0,6046
Adjusted R square						0,6045
Absolute Sum of Squares		1771000	914707	3137000	972889	6796000
Sy.x						24,07
Normality of Residuals						
D'Agostino & Pearson omnibus K2		207,7	218,4	388,5	1120	
P value	< 0.0001	< 0.0001	< 0.0001	< 0.0001		
Shapiro-Wilk W		0,9525	0,9408	0,8994	0,8431	
P value	< 0.0001	< 0.0001	< 0.0001	< 0.0001		
Kolmogorov-Smirnov distance		0,0977	0,1344	0,1505	0,1566	
P value	< 0.0001	< 0.0001	< 0.0001	< 0.0001		
Replicates test for lack of fit						
SD replicates						23,05
SD lack of fit						28,61
Discrepancy (F)						1,54
P value					< 0.0001	
Evidence of inadequate model?					Yes	
Covariance Matrix						
Y0 & Plateau		0,6415	0,6415	0,6415	0,6415	0,6415
Y0 & K		-0,7307	-0,7307	-0,7307	-0,7307	-0,7307
Plateau & K		-0,9865	-0,9865	-0,9865	-0,9865	-0,9865
Dependency						
Y0		0,7689	0,7689	0,7689	0,7689	0,7689
Plateau		0,9867	0,9867	0,9867	0,9867	0,9867
K		0,9895	0,9895	0,9895	0,9895	0,9895
Constraints						
Y0	Y0 is shared	Y0 is shared	Y0 is shared	Y0 is shared		
Plateau	Plateau is shared	Plateau is shared	Plateau is shared	Plateau is shared		
K	K > 0.0 and shared	K > 0.0 and shared	K > 0.0 and shared	K > 0.0 and shared		
Number of points						
Analyzed		2934	2934	2934	2934	
Outliers (not excluded, Q=1.0%)		47	0	262	0	

UNPAIRED T TEST RESULTS, CONTROLS GROUP VS CONCURRENT MODALITY TREATMENT GROUP

P value and statistical significance:

The two-tailed P value is less than 0.0001

Confidence interval:

The mean of Group One minus Group Two equals 32.30000

95% confidence interval of this difference: From 32.00292 to 32.59708

Intermediate values used in calculations:

t = 213.6134

df = 5860

standard error of difference = 0.151

Group	Group One	Group Two
Mean	166.90000	134.60000
SD	5.25600	6.27600
SEM	0.09708	0.11592
N	2931	2931

Post hoc analyses: cediranib monotherapy vs concurrent modality treatment group

UNPAIRED T TEST RESULTS, CONTROLS GROUP VS CONCURRENT MODALITY TREATMENT GROUP

P value and statistical significance:

The two-tailed P value is less than 0.0001

Confidence interval:

The mean of Group One minus Group Two equals 15.90000
95% confidence interval of this difference: From 15.56601 to 16.23399

Intermediate values used in calculations:

t = 93.5325
df = 6398
standard error of difference = 0.170

Group	**Group One**	**Group Two**
Mean	150.50000	134.60000
SD	7.28600	6.27600
SEM	0.12880	0.11095
N	3200	3200

UNPAIRED T TEST RESULTS CONTROLS VS CEDIRANIB MONO

P value and statistical significance:

The two-tailed P value is less than 0.0001

Confidence interval:

The mean of Group One minus Group Two equals 16.40000
95% confidence interval of this difference: From 16.04698 to 16.75302

Intermediate values used in calculations:
t = 91.2739
df = 4998
standard error of difference = 0.180

Group	Group One	Group Two
Mean	166.90000	150.50000
SD	5.25600	7.28600
SEM	0.10512	0.14572
N	2500	2500

DESCRIPTIVES CONTRAST INTENSITIES 1'30"-2'00"

Descriptive Statistics

	N	Minimum	Maximum	Mean	Std. Deviation
Controlspeak	3312	86,70	209,13	127,2156	28,34153
Cediranibpeak	3198	55,91	151,93	89,1489	20,62063
Radiotherapypeak	3312	43,09	139,42	101,4872	28,46857
ConcurrentTherapypeak	3312	51,99	144,97	87,0306	18,25251
Valid N (listwise)	3198				

Tests of Normality

	Kolmogorov-Smirnov[a]			Shapiro-Wilk		
	Statistic	df	Sig.	Statistic	df	Sig.
Controlspeak	,227	3198	,000	,810	3198	,000
Cediranibpeak	,138	3198	,000	,928	3198	,000
Radiotherapypeak	,159	3198	,000	,850	3198	,000
ConcurrentTherapypeak	,125	3198	,000	,950	3198	,000

a. Lilliefors Significance Correction

INDUCTIVES CONTRAST INTENSITIES 1'30"-2'00"

KRUSKAL-WALLIS ONE WAY ANALYSIS OF VARIANCE ON RANKS WOENSDAG, APRIL 06, 2016, 20:03:23

Data source: Data 1 in Notebook1

Normality Test (Kolmogorov-Smirnov): Failed (P < 0,050)

Group	N	Missing	Median	25%	75%
Col 1	3312	0	122,035	109,283	129,220
Col 2	3198	0	82,140	77,453	97,080
Col 3	3312	0	108,620	91,773	120,527
Col 4	3312	0	84,890	70,150	101,530

H = 4228,038 with 3 degrees of freedom. (P = <0,001)

The differences in the median values among the treatment groups are greater than would be expected by chance; there is a statistically significant difference (P = <0,001)

To isolate the group or groups that differ from the others use a multiple comparison procedure.

All Pairwise Multiple Comparison Procedures (Dunn's Method) :

Comparison	Diff of Ranks	Q	P	P<0,050
Col 1 vs Col 4	5317,026	57,066	<0,001	Yes
Col 1 vs Col 2	5028,539	53,495	<0,001	Yes
Col 1 vs Col 3	2565,353	27,533	<0,001	Yes
Col 3 vs Col 4	2751,674	29,533	<0,001	Yes
Col 3 vs Col 2	2463,186	26,204	<0,001	Yes
Col 2 vs Col 4	288,488	3,069	0,013	Yes

Note: The multiple comparisons on ranks do not include an adjustment for ties.

MANN-WHITNEY RANK SUM TEST CONTROLS VS RADIOTHERAPY GROUP DINSDAG, MAART 29, 2016, 15:31:53

Data source: Data 1 in Notebook1

Normality Test (Kolmogorov-Smirnov): Failed (P < 0,050)

Group	N	Missing	Median	25%	75%
Col 1	3313	1	122,035	109,284	129,222
Col 13	3313	1	108,618	91,771	120,528

Mann-Whitney U Statistic= 3327267,500

T = 13128404,500 n(small)= 3312 n(big)= 3312 (P = <0,001)

The difference in the median values between the two groups is greater than would be expected by chance; there is a statistically significant difference (P = <0,001)

DESCRIPTIVES CONTRAST INTENSITIES 15'00"-15'30"

Descriptive Statistics

	N	Minimum	Maximum	Mean	Std. Deviation
Controls	3312	78,39	219,71	118,6723	31,58578
Cediranib	3312	42,40	108,64	72,2745	11,10678
Radiotherapy	3312	73,89	139,04	107,2420	15,81605
ConcurrentModality	3312	52,63	131,11	90,7373	20,80737
Valid N (listwise)	3312				

Tests of Normality

	Kolmogorov-Smirnov[a]			Shapiro-Wilk		
	Statistic	df	Sig.	Statistic	df	Sig.
Controls	,180	3312	,000	,867	3312	,000
Cediranib	,060	3312	,000	,974	3312	,000
Radiotherapy	,176	3312	,000	,915	3312	,000
ConcurrentModality	,113	3312	,000	,934	3312	,000

a. Lilliefors Significance Correction

INDUCTIVES CONTRAST INTENSITIES 15'00"-15'30"

KRUSKAL-WALLIS ONE WAY ANALYSIS OF VARIANCE ON RANKS WOENSDAG, APRIL 06, 2016, 19:49:34

Data source: Data 1 in Notebook1

Normality Test (Kolmogorov-Smirnov): Failed (P < 0,050)

Group	N	Missing	Median	25%	75%
Col 1	3312	0	107,830	90,852	136,058
Col 2	3312	0	72,940	62,732	79,205

Col 3	3312	0	111,510	92,490	118,558
Col 4	3312	0	96,050	77,662	104,988

H = 6129,698 with 3 degrees of freedom. (P = <0,001)

The differences in the median values among the treatment groups are greater than would be expected by chance; there is a statistically significant difference (P = <0,001)

To isolate the group or groups that differ from the others use a multiple comparison procedure.

All Pairwise Multiple Comparison Procedures (Dunn's Method) :

Comparison	**Diff of Ranks**	**Q**	**P**	**P<0,050**
Col 1 vs Col 2	6566,920	69,874	<0,001	Yes
Col 1 vs Col 4	3215,290	34,212	<0,001	Yes
Col 1 vs Col 3	551,378 5,867		<0,001	Yes
Col 3 vs Col 2	6015,542	64,007	<0,001	Yes
Col 3 vs Col 4	2663,912	28,345	<0,001	Yes
Col 4 vs Col 2	3351,630	35,662	<0,001	Yes

Note: The multiple comparisons on ranks do not include an adjustment for ties.

MANN-WHITNEY RANK SUM TEST CEDIRANIB MONOTHERAPY VS CONCURRENT MODALITY TREATMENT GROUP DINSDAG, MAART 29, 2016, 14:07:11

Data source: Data 1 in Notebook1

Normality Test (Kolmogorov-Smirnov): Failed (P < 0,050)

Group	**N**	**Missing**	**Median**	**25%**	**75%**
Col 1	3312	0	72,940	62,732	79,205
Col 2	3312	0	96,050	77,662	104,988

Mann-Whitney U Statistic= 2551155,500

T = 8037483,500 n(small)= 3312 n(big)= 3312 (P = <0,001)

The difference in the median values between the two groups is greater than would be expected by chance; there is a statistically significant difference (P = <0,001)

MANN-WHITNEY RANK SUM TEST CONTROLS VS CONCURRENT MODALITY TREATMENT GROUP DINSDAG, MAART 29, 2016, 15:31:53

Data source: Data 1 in Notebook1

Normality Test (Kolmogorov-Smirnov): Failed (P < 0,050)

Group	N	Missing	Median	25%	75%
Col 1	3313	1	122,035	109,284	129,222
Col 13	3313	1	108,618	91,771	120,528

Mann-Whitney U Statistic= 3327267,500

T = 13128404,500 n(small)= 3312 n(big)= 3312 (P = <0,001)

The difference in the median values between the two groups is greater than would be expected by chance; there is a statistically significant difference (P = <0,001)